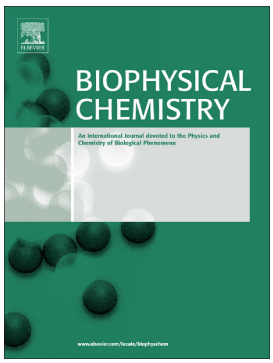

A rationally designed synthetic antimicrobial peptide against Pseudomonas-associated corneal keratitis: Structure-function correlation

Sk Abdul Mohid, Prerana Sharma, Amani Alghalayini, Tripti Saini, Debarun Datta, Mark D.P. Willcox, Haydar Ali, Sreyan Raha, Achintya Singha, DongKuk Lee, Nirakar Sahoo, Charles G. Cranfield, Sanhita Roy, Anirban Bhunia

PII: S0301-4622(22)00044-8

DOI: https://doi.org/10.1016/j.bpc.2022.106802

Reference: BIOCHE 106802

To appear in: *Biophysical Chemistry*

Received date: 28 January 2022

Revised date: 10 March 2022

Accepted date: 15 March 2022

Please cite this article as: S.A. Mohid, P. Sharma, A. Alghalayini, et al., A rationally designed synthetic antimicrobial peptide against Pseudomonas-associated corneal keratitis: Structure-function correlation, *Biophysical Chemistry* (2021), https://doi.org/10.1016/j.bpc.2022.106802

A Rationally Designed Synthetic Antimicrobial Peptide Against *Pseudomonas*-associated Corneal Keratitis: Structure-Function Correlation

Sk Abdul Mohid[1], Prerana Sharma[2], Amani Alghalayini[3], Tripti Saini[4], Debarun Datta[5, 6], Mark D P Willcox[5], Haydar Ali[7], Sreyan Raha[8], Achintya Singha[2], DongKuk Lee[9], Nirakar Sahoo[4], Charles G. Cranfield[3], Sanhita Roy[2], and Anirban Bhunia[1,]*

[1]Department of Biophysics, Bose Institute, Kolkata 700091, India,

[2]L V Prasad Eye Institute, Hyderabad- 500034, India,

[3]School of Life Science, University of Technology Sydney, Ultimo NSW 2007, Australia,

[4]Department of Biology, The University of Texas Rio Grande Valley, Edinburg, TX 78539, USA,

[5]School of Optometry and Vision Science, University of New South Wales, Sydney, Australia,

[6]Optometry and Vision Science Research Group, Aston University, UK,

[7]Indian Association for the Cultivation of Science, Jadavpur, Kolkata 700032. India,

[8]Department of Physics, Bose Institute, Kolkata 700009, India,

[9]Seoul National University of Science and Technology, Seoul 01811, Korea,

*Corresponding E-mail: anirbanbhunia@gmail.com / bhunia@jcbose.ac.in

ABSTRACT

Contact lens wearers are at an increased risk of developing *Pseudomonas*-associated corneal keratitis, which can lead to a host of serious ocular complications. Despite the use of topical antibiotics, ocular infections remain a major clinical problem, and a strategy to avoid *Pseudomonas*-associated microbial keratitis is urgently required. The hybrid peptide VR18 (VARGWGRKCPLFGKNKSR) was designed to have enhanced antimicrobial properties in the fight against *Pseudomonas*-induced microbial keratitis, including contact lens-related keratitis. In this paper, VR18's modes of action against *Pseudomonas* membranes were shown by live cell Raman spectroscopy, live cell NMR, live-cell fluorescence microscopy and measures taken using sparsely tethered bilayer lipid membrane bacterial models to be via a bacterial-specific membrane disruption mechanism. The high affinity and selectivity of the peptide were then demonstrated using *in vivo*, *in vitro* and *ex vivo* models of *Pseudomonas* infection. The extensive data presented in this work suggests that topical employment of the VR18 peptide would be a potent therapeutic agent for the prevention or remedy of Pseudomonas-associated microbial keratitis.

KEYWORDS

Contact Lens • Bacterial keratitis • antimicrobial peptide (AMP) • Nuclear magnetic resonance (NMR) • *Pseudomonas aeruginosa.*

INTRODUCTION

Corneal opacity is the fifth leading cause of blindness globally, accounting for ~3.2% of all cases.[1 2] The recent World Health Organisation (WHO) report highlighted that ~6 million of the world's population are affected by cornea-related blindness or moderate/ severe visual impairment, including 2 million of those who are affected by trachoma.[3] Infectious keratitis is considered a "silent epidemic" in the western world, with an annual incidence on the order of 25,000-30,000 in the US alone.[4] Being more abundant in developing countries, infectious keratitis has been designated as a "neglected tropical disease". To date, antibiotics like vancomycin, tobramycin and amphotericin B (AmB) are the best choices for treating microbial keratitis.[5] These drugs, however, are toxic to mammalian cells and cause membrane disruption, interruption of physiological ion transport, neurotoxicity and nephrotoxicity.[6] On the other hand, the emergence of several multidrug-resistant bacteria is causing all new antibiotics to fail.[7]

The last few decades have seen the rise of antimicrobial peptides (AMPs) as potent alternatives to the available therapeutic agents, owing to their species specificity.[8] The predilection for the lipid environment is a common trait of membrane-active peptides.[9] They are mostly unstructured in solution and, in the presence of lipid membranes, it is thought they will adsorb onto the surface via electrostatic interactions, alter secondary structure, then intrude into the hydrophobic core of the membrane bilayer and destroy bilayer stability.[9, 10] The molecular process by which these membrane-active peptides lyse membranes is defined by several models like barrel-stave, toroidal pore, carpet or detergent mechanisms.[8, 11] In previous studies, we have demonstrated the feasibility of engineering short peptides that specifically disrupt the structural integrity of bacterial and fungal cell membranes but do not interact with mammalian cell membrane components.[12] The VR18 peptide is a chimera consisting of a portion of the dengue viral fusion

peptide and a portion of the lactoferrampin peptide that includes a lipopolysaccharide KNKSR binding motif. Thus, VR18 was explicitly designed to interact with lipopolysaccharides (LPS) and then to disrupt the lipid outer membrane of bacteria leading to cytoplasm leakage and bacterial death.[13]

Here, using live-cell NMR, high-end microscopy, interactions with sparsely tethered lipid bilayer membranes and live-cell Raman spectroscopy, we confirm that VR18's actions are membrane-mediated. We then further show that VR18 reduced *Pseudomonas*-associated keratitis in mice and in *ex vivo* human corneal infection models. Finally, we conclude that the topical application of VR18 could be used as an effective therapeutic agent for combating *Pseudomonas*-associated corneal infections.

MATERIALS AND METHODS

REAGENTS:

The *P. aeruginosa* serotype 10 lipopolysaccharide (LPS), polymyxin B, calcein, and propidium iodide (PI) were purchased from *Sigma Aldrich Co*. (St. Louis, USA.). Deuterium oxide was purchased from *Cambridge Isotope Laboratories, Inc.* (Tewksbury, USA). The bacterial media was purchased from *Himedia Laboratories Pvt. Ltd*., Mumbai, India. 1-palmitoyl, 2-oleoyl-phosphatidylethanolamine (POPE) and 1-palmitoyl, 2-oleoyl-phosphatidylglycerol (POPG), 3-(cholamido-propyl) dimethylammonio-2-hydroxy-1-propane-sulfonate (CHAPSO) and *Escherichia coli* total lipid extract (*E. coli* TLE) were obtained from *Avanti Polar Lipids* (Alabaster, AL).

PEPTIDE SYNTHESIS:

^{15}N labeled VR18 was synthesized by Fmoc solid-phase peptide synthesis chemistry, as described previously, using an automated peptide synthesizer (Aapptec Endeavor 90, Louisville, KY, USA).[13, 14] The Val-1, Ala-2, Gly-4, Gly-6, Leu-11 and Gly-13 residues were selectively labeled with ^{15}N by using the ^{15}N labeled Fmoc-amino acids, respectively. N-terminal Val-1 residue was subjected to acetylation in order to provide protection during the peptide cleavage step. The crude peptide was purified by a reverse-phase high performance liquid chromatographic system (RP-HPLC) (LC-20AT, SHIMADZU, Kyoto, Japan) using a Phenomenix C_{18} column. The peptide fraction was collected from the RP-HPLC elution and subjected to lyophilization to obtain the powder form. The calculated and actual molecular weight obtained for the peptides was 2107.49 and 2107.26, respectively. The purified peptide (>95% purity) was stored at -20°C.

DETERMINATION OF MINIMAL INHIBITORY CONCENTRATION:

To determine the $MIC_{99\%}$, a modified micro broth dilution assay was done, as previously described.[12] In brief, the mid-log phase cultures of *P. aeruginosa* 6294 was pelleted down by centrifuging at 8000 rpm for 10 minutes, washed twice with 10 mM Sodium phosphate buffer, pH 7.4 and re-suspended in the same buffer to get a final cell suspension containing 10^5 CFU/ml. The exposure to the peptide was set with 50 µl of this cell suspension being added to a series of concentrations of the VR18 peptide (ranging from 1 to 100 µM diluted from a 1 mM stock solution) in a sterile 96-well micro titter polypropylene plate and incubated for 3 h at 37 ℃. A positive control containing only cells and a negative control containing 10 µM Polymyxin B treated cells were also maintained. Following peptide exposure, 200 µl of nutrient broth was added to each well and incubated overnight at 37 ℃. Absorbance of each well was measured at 630 nm to estimate $MIC_{99\%}$ of each peptide. The $MIC_{99\%}$ was defined as the lowest concentration

that inhibited 99% growth of the microorganisms from initial microbial cell density. All experiments were set in triplicates.

ZETA POTENTIAL ANALYSIS

Overnight grown log phase cultures of *P. aeruginosa* 6294 in nutrient broth, were washed twice and resuspended in 10 mM phosphate buffer of pH 7.4. 1 ml cell suspension of 10^5 cells per ml and were subsequently incubated with 1-15 µM VR18 peptide for 90 min. The same microbial suspension without the peptide was used as the negative control set and a 10 µM Polymyxin B treated cell suspension was used as a positive control. All of these suspensions were placed in disposable zeta cells and read at 25 °C using a Nano S ZEN3690 (Malvern Instruments, Westborough, MA). The zeta potential for each sample was calculated using the Zetasizer software.[15]

PROPIDIUM IODIDE UPTAKE ASSAY

Mid-log phase of *P. aeruginosa* 6294 cells ($O.D_{630}$ 0.5) obtained from an overnight culture nutrient broth were pelleted by centrifugation at 8000 rpm for 10 minutes at 25 °C, washed twice with 10 mM phosphate buffer (pH 7.4) and resuspended in the same buffer. propidium iodide (PI), a nucleic acid binding dye, was added to 50 µl of the cells with a concentration of 10 µM and allowed to stabilize for 30 minutes. The intensity of the PI bound with intact cells was measured using the time kinetics mode of the spectrometer. An increasing concentration of the VR18 peptide was added to the cell after 10 minutes and the increase in PI fluorescence due to outer and inner membrane permeabilization was measured using a Hitachi F-7000FL spectrophotometer. The excitation wavelength was set at 580 nm and the emission was recorded at 620 nm with a slit width of 5 nm.

RAMAN SPECTROSCOPY

The *P. aeruginosa* 6294 cells were processed in a similar way to the zeta potential sample preparation and treated with the peptide at 1x and 2x MIC concentrations. The cell suspensions were then drop-casted onto clean aluminum foil mounted on the glass slide.[16] Raman spectra were obtained in backscattering geometry using a LabRAM HR - Jobin Yvon (Horiba, Kyoto, Japan) spectrometer equipped with a Peltier-cooled CCD.[16] A diode laser of wavelength 785 nm was used as an excitation source, and the light was focused on the sample using a 50× objective. All data were recorded within a wavenumber range from 800 to 1300 cm^{-1}.

For curve fitting, the *Origin* program was used. First, the baseline of the Raman spectra was processed by asymmetric least squares (ALS) method. The parameter for the asymmetric factor was kept 0.001, while keeping the threshold, smoothing factor and number of iterations at 0.05, 4 and 10, respectively. To reduce the noise and to get a clearer picture of the Raman shifts, further smoothening of the data was done by using Savitzky-Golay methods where the points of window were kept to 25 and the polynomial order was set at 5 without any boundary condition. The specific and significant Raman shifts of the different chemical groups and bonds were matched with a previously reported article by GB Jung et al.[17]

PREPARATION OF UNILAMELLAR VESICLES

Approximately 2 mg each of 1-palmitoyl, 2-oleoylphosphatidylethanolamine (POPE) and 1-palmitolyl, 2-oleoylphosphatidylglycerol (POPG) were dissolved in chloroform with molar ratio of 3:1 (mimicking the bacterial inner membrane composition). The solvent was then evaporated

by passing N2 gas and then lyophilized overnight. Thereafter, the film was hydrated with 10 mM Tris buffer (pH-7.4) containing 70 mM calcein (Sigma, St. Louis, USA). Then the mixture was subjected to five freeze–thaw cycles in liquid N2 and heated to 60 °C along with vigorous vortexing. Large Unilamellar vesicles (LUV) of 100 nm were created by passing the mixture 25 times through a polycarbonate filter (pore size 100 nm) attached with an extruder (Avanti Polar Lipids, Alabaster, Alabama) at 25 °C. Free calcein was separated by passing the solution through a Sephadex G-50 column (GE Healthcare, Uppsala, Sweden) at 25 °C with Tris buffer as eluent.

CALCEIN DYE LEAKAGE ASSAY

The leakage of calcein was monitored on a Hitachi F-7000FL spectrophotometer by setting the excitation wavelength at 495 nm, and the wavelength scan showed the emission maxima at 517 nm from the LUV dispersion (20 μM lipid in 10 mM Tris with 100 mM NaCl, pH 7.4) as described previously.[18] 1 % Triton X100 was used as a positive control and the percentage of leakage was calculated as the following:

Percentage of calcein leakage = $(F - F_0) / (F_T - F_0) \times 100$

Where,

F = the calcein fluorescence emission maximum at a certain concentration of peptides.

F_0 = the calcein fluorescence emission without the addition of peptide.

F_T = the calcein fluorescence emission in presence of 1% Triton X100.

Each experiment was done in triplicate at 37 °C

PHASE CONTRAST MICROSCOPIC ANALYSIS

Unlabeled giant unilamellar vesicles (GUVs) were prepared by following the gel-assisted method as described by Weinberger et al. and modified as per requirements.[19] Briefly, a solution of 5% (w/w) poly-vinyl alcohol (PVA) was prepared by dissolving into Millipore water and heated at 90 ℃ with constant stirring until the suspension become a clear solution. 300 µl of the solution was then dropped in a small 30 mm petri dish to make a thin even layer. The plates were then transferred into a hot air oven and kept for drying at 50 ℃ for 30 minutes.

For phase contrast microscopy, stock solutions of 2 mg/ml POPE, and POPG were prepared in chloroform and 20 µl of the lipid mixture (prepared by maintaining the particular ratios) were spread on the PVA film in a non-overlapping way. Then, the plates were placed in a Lyophilizer for 45 minutes to remove the trace amount of the solvents. Before using the lipid films, the plates were subjected to UV treatment for 15 minutes to prevent dewetting and cleaning. To create a phase difference while observing the GUVs under the microscope, 800 µl of 100 mM sucrose solution was added into the lipid film to swell the GUVs for 10-15 minutes.[20] Then the plates were gently swirled to dislodge the vesicles from the PVA layer and thereafter, the GUVs were collected in a polypropylene microcentrifuge tube within 45 minutes. Next, the vesicles were added into a well where a 105 mM glucose solution was already added, with or without the peptide solution. The GUVs were imaged using a Nikon model Ts2FL microscope (Nikon, Japan).[20]

SPARSELY TETHERED BILAYER LIPID MEMBRANES (STBLMS).

To measure how the VR18 peptide interacts with lipid bilayers, sparsely tethered bilayer lipid membranes (stBLMs) in conjunction with swept frequency electrical impedance spectroscopy (EIS) was used.[21, 22] Changes in membrane conduction and membrane capacitance were

measured in the presence of increasing concentrations of the VR18 peptide on membranes containing either three parts 1-palmitoyl-2-oleoyl-glycero-3-phosphotidylethanolomine (POPE) with 1 part 1-palmitoyl-2-oleoyl-glycero-3-phosphotidyleglycerol (POPG); or as a 60% palmitoyl-2-oleoyl-glycero-3-phosphotidylcholine (POPC) mixture with 40% cholesterol (Avanti Lipids, USA).[23]

To create the stBLMs, a first layer of anchoring lipids consisting of tethered benzyl-disulfide (tetra-ethyleneglycol) n = 2 C20-phytanyl '*tethers*' with benzyl-disulfide-tetra-ethyleneglycol-OH '*spacers*' in the ratio of 1:10 (SDx Tethered Membranes Pty Ltd, Australia) was incubated with gold patterned polycarbonate slides for one hour. These were then washed with 100% ethanol and kept in sealed storage, in the presence of ethanol, until needed. Prior to use, these chemically coated electrode slides were attached to a TethaPlate™ cartridge[22] before the addition of 8 µL of a 3 mM solution of the select mobile lipids in 100% ethanol. These were then incubated with the tethering chemistry for exactly 2 minutes before being solvent exchanged with 3 x 400 ml of a buffer containing 10 mM Tris, 100 mM NaCl at pH = 7.4.

EIS measures were obtained using a 50-mV peak-to-peak swept-frequency AC excitation from 2000 Hz to 0.1 Hz with four steps per decade. Phase and impedance data were recorded using a TethaPod™ operated with TethaQuick™ software (SDx Tethered Membranes Pty Ltd, Australia). An equivalent circuit consisting of a Resistor/Capacitor network to represent the lipid bilayer membrane in series with a *Constant Phase Element* (CPE), to represent the imperfect capacitance of the gold tethering electrode, and a resistive element to represent the electrolyte conductance, was applied to fit the collected impedance and phase data, as described previously.[23] A proprietary adaptation of a Lev Mar fitting routine was used to obtain the optimal goodness of fit. The data were normalized to baseline conduction and capacitance values directly

before the addition of each compound to account for variations in basal membrane conditions due to the differing membrane lipid mixtures.

Changes in membrane conduction were then measured as a result of adding 150 µl of VR18 peptide in increasing concentrations ranging from 1 µM – 100 µM, with a 3 x 400 µl buffer wash step between each peptide addition.

ISOTHERMAL TITRATION CALORIMETRY ANALYSIS

Isothermal titration calorimetry (ITC) was performed to determine the thermodynamic parameters of binding of VR18 peptide with *P. aeruginosa* LPS micelles using a TA-affinity ITC (TA instruments, Bangalore, IN). All reagents and peptides were dissolved in 10 mM phosphate buffer at pH 7.4 and degassed. A sample cell (volume 182 µl) containing 0.5 mM VR18 peptide was titrated against *P. aeruginosa* LPS from a stock solution of 0.025 mM at 298 K. A total of 20 injections were carried out at an interval of 2 minutes with 1µL of LPS aliquots per injection. The raw data was plotted using Nano Analyze 3.7.5 software supplied with the instrument. An independent model was used to analyze the dissociation constant (K_d), and the change in the heat of enthalpy of interaction (ΔH), free energy of binding (ΔG) and entropy (ΔS) were evaluated using the equations $\Delta G = -RT \ln K_d$ and $\Delta G = \Delta H - T\Delta S$, respectively.

CIRCULAR DICHROISM ANALYSIS

Circular Dichroism (CD) of VR18 peptide was done in *P. aeruginosa* LPS. The spectra were recorded in a Jasco J-815 spectrophotometer (Jasco International Co., Ltd. Tokyo, Japan) equipped with a Peltier cell holder and temperature controller unit accessory. Stock solutions of

peptide and LPS were prepared in 10 mM phosphate buffer (pH 7.4). The CD data was obtained at 28 °C in a 0.5 cm Quartz cuvette using the final concentration of peptide set at 25 μM and titrating with increasing concentration of LPS (12.5-50 μM) micelles. The spectral range was set at 190 to 260 nm with 1 nm data pitch and averaging 3 accumulations. The buffer subtracted spectral data obtained in milli degrees were converted to molar ellipticity (θ) (deg cm^2 $dmol^{-1}$), using equation (1), where m_0 is milli degrees, M is the molecular weight (g mol^{-1}), L is the path length of the cuvette (cm) and C is the concentration (g L^{-1}).[24]

$$\text{Molar ellipticity } (\theta) = m_0 M/10 \times L \times C \quad (1)$$

NMR EXPERIMENTS

All solution NMR experiments were done at 298 K on a Bruker Avance III 500 MHz equipped with a 5 mm SMART probe and 700 MHz NMR spectrometer equipped with a 5 mm RT probe. NMR samples were prepared in 10% deuterated water (pH 4.5) and 3-(Trimethylsilyl)propionic-2,2,3,3-d4 acid (TSP) sodium salt was used as an internal standard (0.00 ppm). Two-dimensional ^1H-^1H total correlation spectroscopy (2D TOCSY) (, and two-dimensional ^1H-^1H Nuclear over Hauser Spectroscopy (2D NOESY) was recorded for the VR18 peptide with a mixing time of 80 ms and 150 ms, respectively and spectral width of 12 ppm in both directions. The number of scans were fixed to 20 and 40 for TOCSY and NOESY experiments, respectively. The recycle delay (D1) for both the experiments was set to 1.5 sec with 456 increments in the t_1, and 2048 data points in the t_2, dimensions along with states time-proportional phase incrementation (TPPI) for quadrature detection in t_1 dimension and excitation-sculpting scheme for water suppression were used to record both the experiments.[12] Next, the interaction of the peptides upon successive titration with *P. aeruginosa* LPS bicelles or *E. coli* total lipid extract (TLE) bicelles were

monitored by 1D proton NMR acquired using an excitation-sculpting scheme for water suppression and the States-TPPI for quadrature detection in the t1 dimension[25]. Consequently, 2D TOCSY and *transferred* NOESY (*tr*NOESY) spectra of the peptide in the context of LPS or *E. coli* TLE bicelles were acquired with 80 ms and 150 ms mixing time, respectively. Data processing and analysis were carried out using Topspin™ v3.1 software (Bruker Biospin, Switzerland) and Sparky[26] software, respectively. LPS and *E. coli* TLE bicelles were made as described previously.[12, 27] Briefly, 2 mg of *P. aeruginosa* serotype 10 LPS or *E. coli* TLE were measured and mixed separately with 1.5 mg of CHAPSO. 10 mM phosphate buffer (pH 7.4) with 150 mM NaCl was used for hydration and the lipid/detergent ratio (q-ratio) was kept between 0.25 to 0.3. After 3 h of hydration, the mixed solution was subjected to five freeze-thaw cycles and used for further assays.

SAMPLE PREPARATION FOR SOLID-STATE NMR

For ^{31}P solid-state NMR, 5 mg/ml of the lipids from the specified ratio were used as previously described.[28] The lipid samples were dried under a stream of nitrogen and then subjected to lyophilization overnight to eliminate any residual solvent. The films were prepared in a small glass vial. The lipid films were hydrated by adding 50 µl Tris buffer (pH 7.4) and were vortexed for 5 min at ambient temperature and freeze-thawed using liquid nitrogen at least five times to ensure the uniform size of the vesicles. The VR18 peptide was added to the buffered vesicle solution at appropriate weight (for either 2 or 4 mol %), and the final volume was adjusted to 100 µl for each solid-state NMR experiment.

LIVE CELL NMR

Live cell 1D ^{1}H NMR experiments were done with 0.5 mM VR18 peptide dissolved in 90% 10 mM Phosphate Buffer (pH-6.5) and 10% D_2O. Overnight stationary phase *P. aeruginosa* 6294 cells were sub cultured to get log phase cells. The cells were then collected by centrifuging at 5500 rpm for 5 minutes and washed twice with the same buffer and a final 600 µl of 1 $O.D_{630}$ cell concentration i was taken for the experiment. First, a free 1D ^{1}H NMR spectrum of the VR18 peptide was obtained in a Bruker Avance III 500 MHz NMR spectrophotometer (equipped with smart probe). Then the peptide was added to the cell. A series of 1D ^{1}H NMR spectra were obtained over 4 h. Cells in the NMR tube were monitored every 15 minutes and mixed thoroughly to stop the sedimentation. New peaks were observed after 5-10 min as a result of the efflux of metabolites. The number of scans was 48 and the recycle delay was 2 seconds for every 1D spectra.

^{31}P SOLID STATE NMR

NMR experiments were performed on an Agilent NMR spectrometer (DD2) operating at the resonance frequency of 699.88 MHz for ^{1}H and 283.31 MHz for ^{31}P and equipped with a 4 mm MAS HXY Solid Probe (Agilent). ^{31}P NMR experiments were performed using a single 90° pulse and 24 kHz TPPM proton decoupling. The π/2 pulse lengths were 6.8 µs for the ^{31}P nucleus. MLVs were kept in a 4 mm Pyrex glass tube, which was cut to fit into the MAS probe, and sealed with parafilm. An Agilent temperature control unit was used to maintain the sample temperature at 25 °C. ^{31}P spectra were collected with 256 scans and a recycle delay of 2 s and referenced externally to 85% phosphoric acid (0 ppm).[28] All the spectra were processed with MestReNova software(Ver 8.1) with 250 Hz line broadening.

NMR DERIVED STRUCTURE CALCULATION

For calculation of the LPS bicelle-bound three-dimensional structure of the peptide, the volume integrals of the respective nuclear Overhauser effect (NOE) cross-peaks were qualitatively differentiated into strong, medium and weak, depending on their intensities in the *tr*NOESY spectra. This information was further transformed to inter-proton upper bound distances of 3.0, 4.0 and 5.0 Å for strong, medium and weak, respectively, while the lower bound distance was fixed to 2.0 Å. The backbone dihedral angles of the peptides, phi (φ) and psi (ψ) were kept flexible (-30° to 120º and 120 º to -120°, respectively) for all non-glycine residues to limit the conformational space. CYANA program *v*2.1 was used for all structure calculations with iterative refinement of the structure based on distance violation.[29] Hydrogen bonding constraints were excluded from structure calculation. The NMR-derived ensemble structures were analyzed using PyMOL and their stereochemistry was checked using Procheck.[30]

CALCULATION OF DYNAMICS OF THE NMR DERIVED STRUCTURE.

The ^{15}N relaxation parameters R_1, R_2 and [^1H]-^{15}N steady-state heteronuclear NOE were measured on the Bruker Avance III 700 MHz NMR spectrometer using 1.0 mM solution of the selectively ^{15}N-labelled VR12 peptide prepared in 90% H_20 and 10% D_2O solution (pH 4.5).[14] Following this, the relaxation experiments were carried out using the two-dimensional sensitivity-enhanced heteronuclear single quantum correlation (HSQC) based pulse sequences. The complete set of R_1, R_2 and hetNOE data sets were recorded at 298 K with 1024 (t2) and 256 (t1) complex data points, respectively, along the ^1H (SW = 12 ppm, offset = 4.701 ppm) and ^{15}N (SW = 22 ppm, offset = 117.5 ppm) dimensions. All these spectra were processed and analyzed using Topspin^{TM} software suite. Each R_1 and R_2 data sets were collected using 8 scans and a recycle delay of 2.5 sec. For R_1 measurements, the following relaxation delays were used: 10, 50, 90, 150, 250, 350, 550, 770, 990 and 1100 ms. For R_2 measurements the following relaxation

delays were used: 0.00, 16.96, 33.92, 50.88, 67.84, 101.76, 135.68, 169.60, and 237.44 ms. The R1 and R2 values with their errors were extracted using MATLAB program "*Relaxation Decay*" developed in MathWorks Inc. Steady-state [^{1}H]-^{15}N heteronuclear NOE (hetNOE) measurements were carried out with a proton saturation time of 3 s and a relaxation delay of 3 s. For the experiment without proton saturation, the relaxation delay was set to 6 s. The NOE intensities for every residue were calculated as I_{sat}/I_{ref}, where I_{sat} and I_{ref} are intensities of the peaks in the HSQC spectra, with and without proton saturation, respectively.

IN VITRO TREATMENT OF HUMAN CORNEAL EPITHELIAL CELLS INFECTED WITH *P. AERUGINOSA* PAO1.

Human corneal epithelial cells (HCECs) (1x10^{4} cells/well) were cultured overnight in 96-well plates at 37 °C and in the presence of 5% CO_2. Cells were infected with *P. aeruginosa* PAO1 at a multiplicity of infection of 10 (Cells: bacteria, 1:10) and incubated in presence or absence of VR18 for 4 h. The viability of *P. aeruginosa* PAO1 was determined by measuring the absorbance at OD_{600}. The bacterial supernatant was then removed, cells were washed twice with 1x PBS and the viability of HCECs were determined by MTT assay.[31]

EX VIVO TREATMENT OF HUMAN CORNEA INFECTED WITH *P. AERUGINOSA* PAO1.

Ex vivo corneas were cleaned and kept in antibiotic-free media for 24 h. Corneas were scratched with a scalpel and infected with 10^{5} cfu/ml of PAO1 (n = 3). 50 µM VR18 peptide was added at the time of infection in 3 other corneas. 24 h post-infection, corneas were washed with PBS and homogenized and plated by serial dilutions and colonies were counted after ON incubation.

MURINE MODELS OF CORNEAL INFECTION.

This study was approved by the Institutional Animal Ethics Committee of the test facility (Institutional Animal Ethics Committee, Vivo Bio Tech Ltd.; Study Number: 18/0077). C57BL/6 mice (6-8 weeks old) were anesthetized by intraperitoneal injection of ketamine (8.7 mg/ml) and xylazine (0.5 mg/ml) at a dose of 0.01 ml/g body weight and the corneal epithelium was abraded with three parallel 1 mm scratches using a 26-gauge needle and separated in two random groups. An aliquot of 3 µl containing approximately $1x10^5$ PAO1 was added topically to one eye, and 1x PBS was added to the fellow eye of one group. To the second group, 5 µl of 50 µM of VR18 was added immediately after the addition of PAO1. The second dose of VR18 was added topically 6 h post-infection to the second group. Mice were euthanized and examined for corneal opacification, ulceration, or perforation 24 h post-infection. Clinical scores for the opacity were determined in a blinded fashion according to a scale earlier reported.[32] To measure colony forming units (CFUs), whole eyes were homogenized in sterile 1x PBS using a tissue homogenizer (Genetix Biotech, Hyderabad, India) and serial dilutions were plated on LB agar plates, and cfu was counted manually. All animals were housed in pathogen-free conditions in microisolator cages and were treated in accordance with the guidelines provided in the ARVO Statement for the Use of Animals in Ophthalmic and Vision research.

REACTIVE OXYGEN SPECIES (ROS) MEASUREMENTS FROM VR18 TREATED *P. AERUGINOSA*.

BACTERIA AND REAGENTS: *P. aeruginosa* 15692GFP strain was grown aerobically in Luria-Bertani (LB) broth at 37 °C overnight. ROS-sensing dye, *CM-H2DCFDA* (2',7'-dichlorodihydrofluorescein diacetate) was obtained from Invitrogen™ Molecular Probes™,

oxidant, terbutyl hydrogen peroxide (tbH_2O_2) was obtained from Fischer scientific, and VR18 peptide was obtained from Genscript.[33]

MEASUREMENT METHOD: ROS measurement was performed at room temperature with the PTI EasyRatioPro system (HORIBA Scientific). Log-phase cultures of *P. aeruginosa* were incubated with 10 µM ROS-sensing dye, *CM-H2DCFDA* in Tyrode's solution (145 mM NaCl, 5 mM KCl, 2 mM $CaCl_2$, 1 mM $MgCl_2$, 10 mM Glucose, and 20 mM HEPES, pH 7.4) for 1 h in the dark. Following incubation, the bacteria were washed twice to remove the excess dye. A small drop of ~30 µl of the bacterial suspension was placed on a glass coverslip and 0.5% agarose pad of 0.7 x 0.7 cm was placed on top of the bacteria. The imaging was performed on an Olympus IX71 inverted microscope attached to PTI EasyRatioPro system. A change in fluorescence was recorded with EasyRatioPro software with an excitation wavelength at 494 nm and an emission wavelength at 520 nm. All the chemicals such as VR18, tbH_2O_2 (1 M) of 5 µl were dropped into the side of the agarose pad during the live measurements to test their effect on the intracellular ROS generation. [34]

RESULTS AND DISCUSSION

Interaction of VR18 with invasive Pseudomonas aeruginosa

We explored the efficiency of VR18 against two invasive *P. aeruginosa* strains (6294 and PAO1) which are widely used for the model organisms for bacterial keratitis studies.[35]

In order to check the *in vitro* activity of VR18, a micro broth dilution assay was prepared by using *P. aeruginosa* 6294. This showed that the VR18 killed the pathogen in a dose-dependent

manner with ~80% and 99% bacterial cell death at 5 μM and 10 μM concentrations, respectively (Figure 1A).

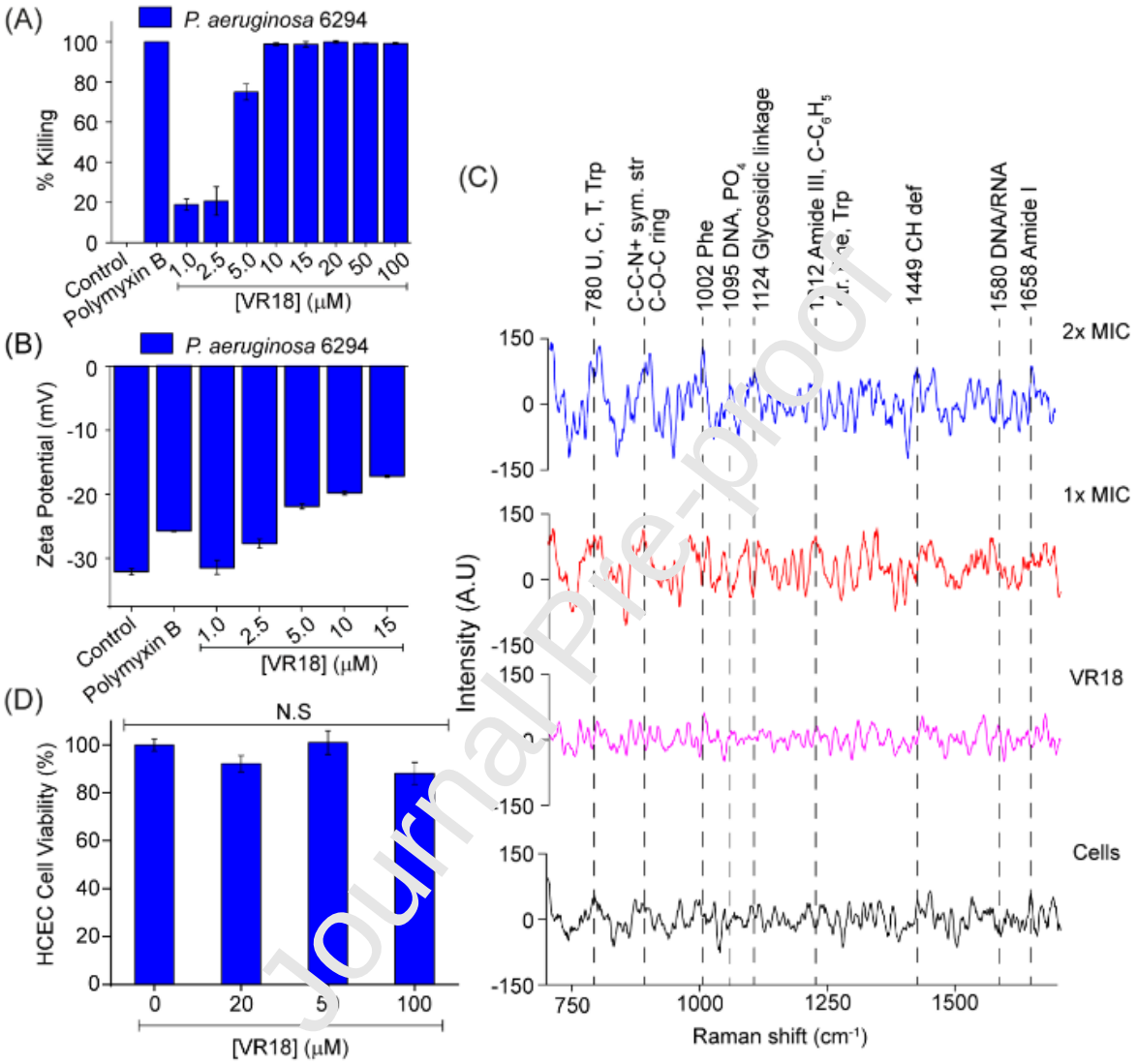

Figure 1. (A) Micro broth dilution assay showing $MIC_{99\%}$ at 10μM concentration of VR18 against *P. aeruginosa* 6294. (B) Measurement of zeta potential of the bacterial cells in presence of different concentration of VR18. (C) the averaged Raman spectra of the free bacteria, free VR18 and the bacteria treated with 1x and 2x MIC of VR18, respectively, showing several peaks which originated from the lysed bacterial cell after the treatment of the peptide. (D) MTT assay of HCEC cells at 2x, 5x and 10x MIC of VR18. The error bars represent the ±SD. N.S- Not significant.

Next, to understand the interaction between the peptide with the *P. aeruginosa* 6294 strain, several biophysical approaches were taken to understand the mechanism of action of VR18. Firstly, the zeta potential of the bacterial membrane was checked in the absence and presence of

the peptide to observe any alterations on the bacterial cell surface. Zeta potential is defined by the electrical potential difference between solid surfaces that are submerged in a colloidal suspension.[15] The surface potential of the bacterial cells play a significant role in the maintenance of the cellular function and also provides useful information about cell surface characteristics.[36] It has been reported that the membrane targeting agents that alter the membrane integrity also changes the zeta potential of the cell surface.[36] This technique can identify the microbial surface targeting agents that act via neutralizing the membrane potential. Previous studies have shown that the Gram-negative microbial cells have a higher negative zeta potential value due to the presence of LPS molecules on their outer membrane.[15] Figure 1B showed the live-cell zeta potential analysis of the *P. aeruginosa* 629 cells at different concentrations of the VR18 peptide. The average surface charge of the bacterial cells in phosphate buffer was around -32 mV in the absence of the peptide. This negativity of the surface potential was decreased sequentially with increasing concentration of the VR18 peptide and became -17.2 mV at 15 μM (1.5x MIC) concentration, which suggests that the peptide actually neutralizes the negatively charged LPS molecules via electrostatic interactions between positively charged Lys and Arg residues. This finding also suggests that the initial binding of the peptide occurs on the bacterial cell surface and not via any passive insertion or ion-channel mediated incorporation into the microbial cells. Of note, 10 μM polymyxin B was used as a positive control because it kills 99% of the microbial cells at this concentration, but it showed -25.8 mV zeta potential, which is less compared to the zeta potential value (-19.8 mV) of VR18 at its 1x MIC concentration. This suggests that the mode of action of polymyxin B and the VR18 peptide are different in the presence of Gram-negative bacterial cells.

To probe the target of the VR18 on the microbial cell surface and to understand the mode of action, propidium iodide (PI) uptake assay was performed.[37] PI, a membrane-impermeable nucleic acid (DNA/RNA) binding fluorescent dye, generally used to differentiate between apoptotic, necrotic, and healthy cells based on membrane integrity.[38] The time-dependent PI uptake assay with live *P. aeruginosa* 6294 cells treated with different concentrations of VR18 (0.25x, 0.5x and 1x MIC) showed a stepwise increment of PI fluorescence intensity which was compared with a positive control, 10 μM polymyxin B (Figure S1A). These data indicate that the outer and inner cell membranes of the bacterial cells were compromised. The polymyxin B, showed a sigmoidal increment of the graph, whereas the peptide exhibited an exponential graph pattern which indicates that the rate of activity of the VR18 peptide is instant and much faster compared to the polymyxin B.

In order to correlate this data, live-cell one dimensional proton (^{1}H) NMR experiment was done by using a 1 mM peptide solution against $1x10^8$ number of *P. aeruginosa* 6294 cells in 10 mM phosphate buffer (pH 6.5) at 25 °C. The high concentration of the peptide (1 mM) caused immediate lysis of the bacterial cells, as shown previsouly,[39] which results in an increasing concentration of cellular metabolite release into the peptide solution. The metabolite peaks of the compromised cells have been observed within 5-10 min as compared to the control spectrum of bacterial cell suspension as well as the spectrum of the free peptide, as shown in Figure S1B. The new peaks from the lysed bacterial cells increased gradually with time (Figure S1B). The above observations indicate that the microbial cell membrane is the primary target for the peptide.

Since the one dimensional NMR experiments suggested that the *P. aeruginosa* cells are getting disrupted in the presence of a higher concentration (1 mM) of VR18 peptide, we further showed that the lytic effect of the VR18 peptide also occurs at its MIC concentration (10 μM). Live cell

Raman spectroscopy was utilized in this case to understand this phenomena. Raman spectroscopy identifies changes in the vibrational and rotational spectra of large molecules.[40] In this study, the effect of the VR18 peptide was investigated against the *P. aeruginosa* 6294 strain. Figure 1C showed the averaged Raman spectra of the free cells, VR18 and the cells treated with 1x and 2x MIC of VR18, respectively. The vibrational bands typical for nucleic acids, proteins, lipids, and carbohydrates are detailed in Table S1.[17] The spectrum of the free peptide did not overlap with the spectrum of the untreated bacterial cells, and peaks of the treated sets were independent of the individual peptide peaks. Several prominent peaks in the VR18 treated cells matched with the vibrational modes of phenylalanine (1002 cm^{-1}) and amide I (1658 cm^{-1}) in proteins. The sharp band at 1449 cm^{-1} which shows CH deformations can be assigned to polysaccharides, lipids as well as proteins, which are all components of bacterial cell membranes. The Raman spectrum obtained from the nucleus of *P. aeruginosa* 6294 cells is characterized by bands at 780 cm^{-1} (uracil, cytosine and thymine), 1095 cm^{-1} (DNA, PO_4^{3-} stretching), and 1574 cm^{-1} (guanine and adenine). The peak at 1124 cm^{-1} could be associated with the stretching vibration from symmetric glycosidic linkages (C-O-C) and the ring breathing mode of polysaccharides or C-C stretching vibrations. The increment of the above-mentioned peak intensities with increasing concentration of the peptide further suggest that the cellular compartment of the bacterial cells is compromised, and the molecules have been released from the microbial cells.

The subsequent concern was to check any adverse effect of the peptide against human corneal epithelial cells (HCEC). An MTT dye reduction assay[41] was done to check the toxicity of the peptide on HCEC in the presence of 2x, 5x and 10x MIC of the VR18.[31] The results show there

are 90% viable HCEC cells at 10x MIC after 4 h exposure, which indicates that the peptide acts selectively on bacterial cells but is not active against human corneal epithelial cells (Figure 1D).

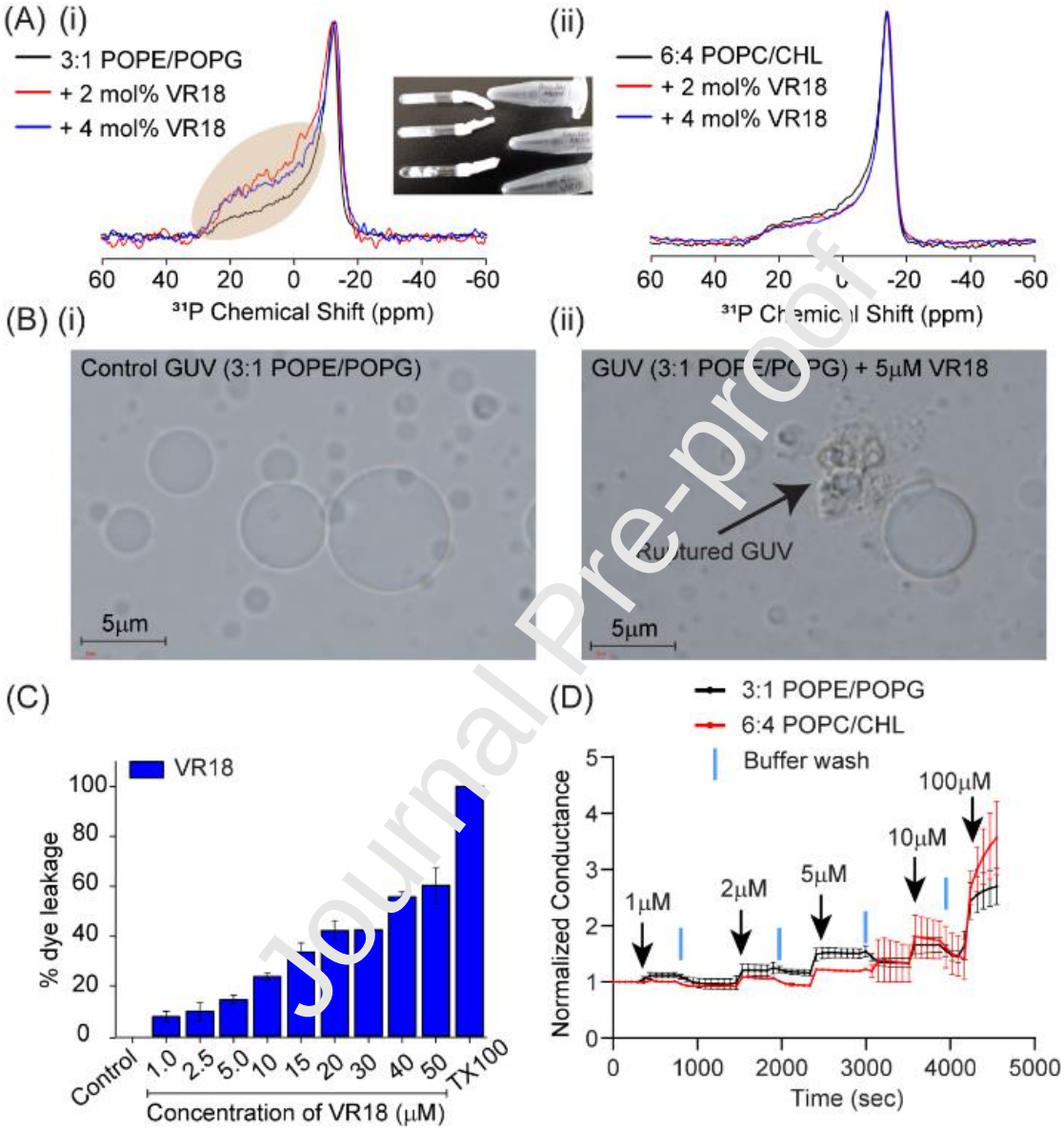

Figure 2. (A) (i) Solid state ^{31}P NMR of the 3:1 POPE/POPG LUVs show immediate thickening of the spectrum at around 0 ppm (marked area). All the ^{31}P NMR spectra were normalized to 1 for the highest peak intensity. (ii) On the contrary, LUVs made of POPC with 40% Cholesterol mimicking the eukaryotic membrane showed no changes. (B) (i-ii) Phase contrast microscopy of GUVs in absence and presence of the VR18 showed bursting of the vesicles with time. (C) Bar graph showing calcein dye leakage assay using the bacterial inner membrane mimicking vesicles. (D) Time-dependent ionic conduction responses in sparsely tethered bilayer lipid membranes composed of 3:1 POPE/POPG and 6:4 POPC/Cholesterol membranes in presence of VR18 peptide. The error bars represent the ±SD of n=3 membranes.

Probing the membrane specificity of the VR18 peptide

To further demonstrate the selective membranolytic nature of the VR18 peptide, model bacterial and eukaryotic membranes were prepared by using 3:1 POPE/POPG and 6:4 POPC/Cholesterol (CHL), respectively (described in the experimental section).[24] Solid-state NMR spectroscopy was employed to monitor the interactions between lipid bilayers and the VR18 peptide by using the ^{31}P nucleus on the phospholipid headgroup. Solid-state ^{31}P NMR spectroscopy is an important technique for studying the different phases formed by model phospholipid membranes.[28] The form of ^{31}P NMR spectrum has different characteristics for different lipid phases, such as gel and liquid crystal lamellar phase, inverted hexagonal phase and isotropic phase (such as small vesicles or micelles).[42] The vesicles composed of 3:1 POPE/POPG and POPC with 40% cholesterol (6:4 POPC/CHL) showed a typical powder pattern of liquid crystal lamellar phase (parallel edge at ~30 ppm and perpendicular edge around -15 ppm) of ^{31}P spectra, as shown in Figure 2A (i-ii) in black line. There was no liquid domain separation, suggesting that the lipids are distributed almost homogeneously in the vesicles of liquid-crystalline Lα phase. Compared to the peptide free spectrum, the spectra of the 3:1 POPE/POPG vesicles with VR18 showed changes in the relative intensities at the parallel edges (~30 ppm) and perpendicular edges (~-15 ppm). This indicates that the peptide interacted with lipids and changed the shape of the vesicles to flattened shape, having an increased number of the lipid molecules of parallel orientation relative to the external magnetic field (Figure 2A (i)). However, no disruption of the vesicle into small vesicles or micelles was observed as there was no isotropic peak obtained at this concentration of the peptide. Surprisingly, the addition of the peptide caused immediate precipitation of the vesicles in the NMR tube as shown in the inset image, which resulted from

increased electrostatic interaction between the peptide and the POPG lipid molecules. This might be the reason to change the ^{31}P spectral shape. On the other hand, the vesicles containing 40% cholesterol showed negligible changes with 2 and 4 mol% peptide as shown in Figure 2A (ii), since the zwitterionic POPC lipid does not interact with the charged peptide. It is noteworthy that the presence of cholesterol molecules also increases the acyl chain order of the vesicles, which subsequently increases its endurance against different AMPs.[43] These observations suggest that the peptide selectively interacted between POPE and POPG lipids due to the electrostatic interaction with oppositely charged headgroups of PG lipids.

The activity of VR18 peptide towards the bacterial model membrane was further examined by the dye release assay and the phase contrast microscopy using Large unilamellar vesicles (LUVs) and Giant unilamellar vesicles (GUVs), respectively, while keeping the same lipid composition as described above. To visualize the lytic action, GUVs filled with 100 mM sucrose solution were employed inside of 105 mM glucose solution to create the phase difference of the incident light in the phase contrast microscope that helps to visualize the vesicles.[20] The addition of VR18 peptide results in a time-dependent burst of the GUVs within 15 minutes of the treatment as compared to the control GUVs (Figure 2B (i-ii)). Likewise, LUVs filled with calcein dye were used to check the dye leakage by using fluorometric analysis. Figure 2C showed a concentration-dependent intensity increment of the calcein dye with 10% to 60% leakage at 1 μM and 50 μM, respectively. This indicates that the peptide is capable of interacting with negatively charged membranes and subsequent disruption increases the free calcein molecules outside the vesicles that increases the intensity of the spectrum. These biophysical studies using model lipid vesicles suggests that the VR18 peptide specifically interacts with the lipid bilayer that mimics the microbial membrane.

In order to gain insight of the lipid-peptide interaction from the electrical properties of the two different membrane models with the VR18, a further analysis was done using sparsely tethered bilayer lipid membranes (stBLMs) in conjunction with electrical impedance spectroscopy.[22, 23] Figure 2D shows a time-course of membrane interactions of the VR18 peptide at increasing concentrations, with subesquent wash steps between each incresaing dose. Relatively small increases in membrane conduction, typical of an alteration in membrane packing, can be seen in both 3:1 POPE/POPG and 6:4 POPC/CHL model membranes in response to the peptide. The membrane conduction does not return to a baseline following each wash step which suggests that the peptide has a slow off-rate - a sign that it has the potential to accumulate at lipid membrane surfaces. It is feasible that this accumulation could be responsible for the lytic activity of the peptide seen in the GUV experiments. At lower concentrations of the peptide (2 – 5 μM), relative conductance changes are greater in the bacterial membrane mimic (3:1 POPE/POPG), suggesting an attraction to these negatively charged lipid headgroups which correlate with the previous findings.

As a Gram-negative bacterium, *P. aeruginosa* has a cytoplasmic membrane with a symmetric phospholipid bilayer and an asymmetric outer membrane with an inner surface of phospholipids and an outer layer that incorporates lipopolysaccharide (LPS), creating a permeation barrier. Since the peptide first interacts with this macromolecule on the microbial cell, isothermal titration calorimetry was done at room temperature to gain insight about the thermodynamic parameters of the interaction between the VR18 and the *P. aeruginosa* LPS. The results shown in Figure S2A and Table S2 suggests that the binding of the peptide with LPS molecules is at micromolar concentration ($K_d = 2.65 \times 10^{-6} \pm 6.46 \times 10^{-7}$ mol/L) and the process is an enthalpy (ΔH) driven mechanism, favouring a spontaneous interaction ($-\Delta G$).

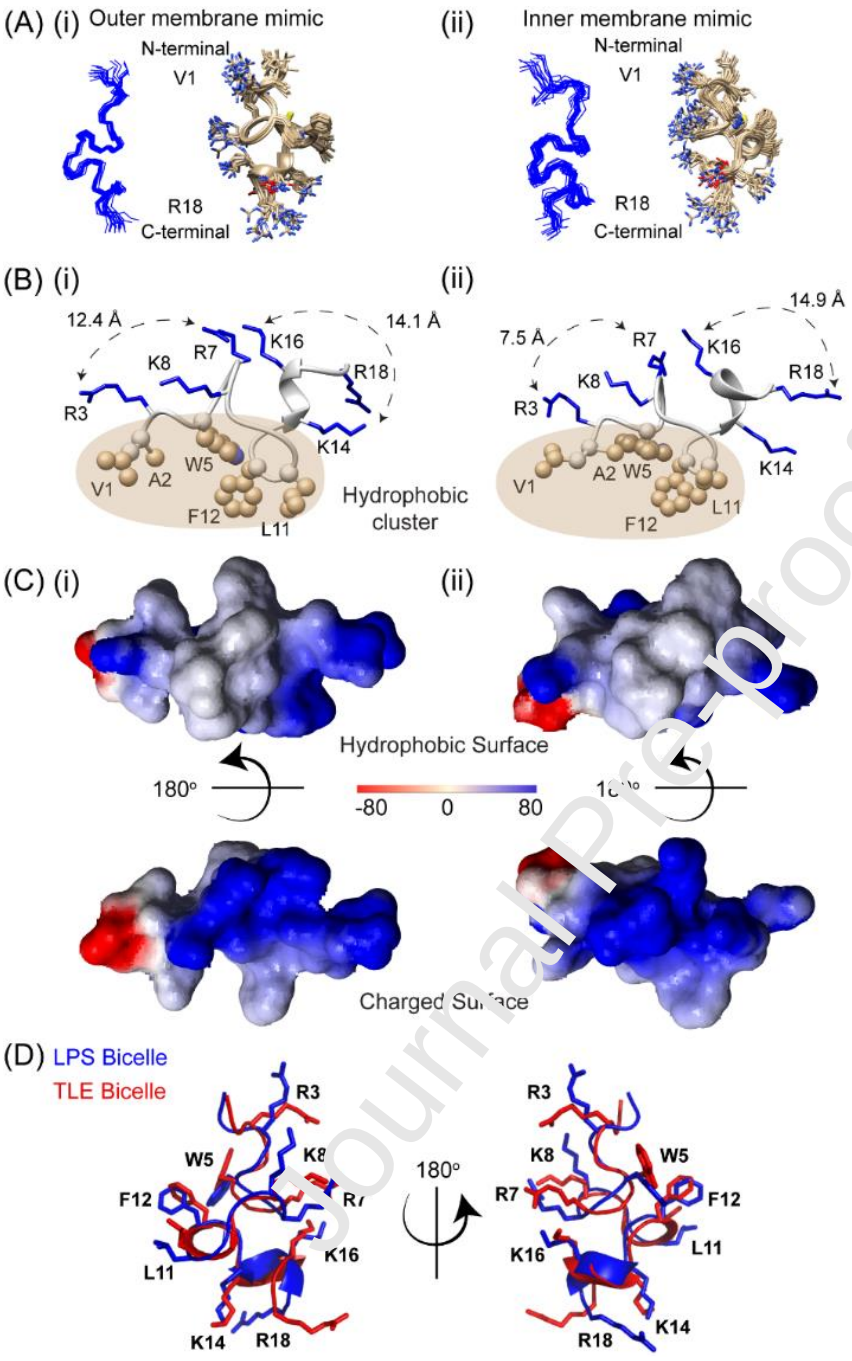

Figure 3. (A-C) Left and right panel shows the LPS bicelle or TLE bicelle bound solution NMR structures of VR18 (PDB IDs: 7VQI and 7VQH). (A) Backbone (Blue) and all states of the 20 ensemble lowest energy structures showing rigid structure with tight backbone packing. (B) Cartoon representation of the single structures showing the separation between charged (blue lines) and hydrophobic (ball and stick model) residues. The positively charged residues maintained a clear separation of 12-15 Å or <10 Å between their hydrophilic head groups, which was comparable to the distance between LPS phosphate head group or PG headgroups (TLE). (C) the electrostatic surface potential of the complex bound to LPS or TLE at an angle of 180° also showed the clear delineation of the surface charge distribution, which was generated with *MOLMOL* software. (D) Overlaid structures of LPS bicelle and TLE bicelle bound VR18 peptide.

Deciphering the atomistic information of the peptide-membrane interaction

To gain insight into structural aspects of the VR18 peptide, high-resolution NMR spectroscopies were performed.[44] Since the K_d value obtained from the ITC experiment was in the micromolar range (K_d ~ 2.65 μM), transferred NOESY (*tr*NOESY) experiments were performed in the presence of bicelles made of *P. aeruginosa* LPS and *E. coli* total lipid extract (TLE). *tr*NOESY is a widely used experiment to determine the conformation and orientation of a ligand bound to a macromolecule.[45] Although the methodology applied may be used to determine the three-dimensional structure of the peptide in the context of a live cell, the release of metabolites within a few minutes of treatment restricted us from employing it in the presence of live *P. aeruginosa* 6294 cells. Instead, bicelles made of *P. aeruginosa* LPS and *E. coli* TLE (composition shown in Table S3) were used to mimic the outer and inner membrane of the bacterial cell, respectively. The NOESY spectra of the free peptide did not exhibit pronounced NOEs except for certain intra- (i, i) or sequential (i, i+1) NOEs, indicating that the free peptide remains highly dynamic (data not shown). This was also confirmed by CD spectroscopy (Figure S2B). Addition of 1-15 ml bicelles to the peptide resulted in concentration-dependent line broadening, without affecting the chemical shift in its one dimensional (1D) proton NMR spectra (data not shown). Similarly, the CD spectra also showed changes in the far UV absorbance, indicating adaptation of the secondary structure in presence of LPS (Figure S2B). Thus, when the free peptide interacts with macromolecules (here bicelles), they undergo a fast to intermediate exchange with the bicelle-bound form under the NMR time-scale. Such a situation is ideal for *tr*NOESY experiments to determine the three-dimensional structure of the peptide in the presence of the bicelles. The *tr*NOESY spectra of the VR18 peptide in presence of the bicelles are summarized in Table S4. A

large number of intra- and sequential (i, i+1) NOEs were observed in both the cases. Several unambiguous medium range (i, i+2/i+3/i+4) NOEs were also observed in between Gly-4/Arg-7, Trp-5/Cys-9, Gly-13/Asn-15 and Gly-13/Lys-16 in the presence of both bicellar systems, except the NOEs between Gly-4α/Gly-6 was observed in case of *P. aeruginosa* LPS bicelle (Figure S3) and Ala-2β/Gly-4 was observed in case of *E. Coli* TLE bicelles (data not shown). This indicates that the peptide gets a folded conformation from random coil structures in presence of the bacterial outer- and inner-membrane environment. Moreover, several long-range NOEs (i, ≥i+5) between Trp-5/Phe-12 and Arg-7/Lys-16 also suggests that the peptide VR18 adopts an amphiphilic structure in the presence of negatively charged membranes (Figure S4).

Using NOE-based distance constraints, we generated 20 ensemble structures of VR18 in *P. aeruginosa* LPS bicelle and *E. coli* TLE bicelle (Figure 3A (i-ii)), demonstrating that the peptide adopts an amphipathic structure by clearly separating positively charged Lys and Arg residues from hydrophobic residues such as Val, Leu, and Phe (Table S4). Closer inspection between the structures highlighted a marked difference between the position of the positively charged residues. The N-terminal Arg-3, Arg-7 and Lys-8 and the C-terminal K14xK16xR18 moiety of the LPS bound structure maintained a distance of 10-15 Å which closely correlates with the distance between two terminal phosphate groups of LPS (Figure 3B, (i)). On the other hand, the C-terminal K14xK16xR18 moiety only maintained a certain distance while the N-terminal Arg-3, Arg-7 and Lys-8 residues stayed closely within 10 Å (Figure 3B, (ii)). The *E. coli* TLE is mainly composed of PE (57.5 wt/wt %) and PG (15.1 wt/wt %) lipids which is why the positively charged residues rearranged themselves in such a way that facilitates the initial electrostatic interaction between the oppositely charged head groups on the bicelle. Of note, two aromatic residues, Trp-5 and Phe-12, maintained a distance of 4.5 - 7 Å while adopting an

energetically favourable T-shaped geometry that stabilized both the structures in the bound form.[12] Apart from that, the non-polar residues consisting of Val-1, Ala-2, Trp-5, Leu-11 and Phe-12 formed a hydrophobic cluster, which is further stabilized by interacting with the acyl chain moieties of the LPS or the lipid molecules in the bicelles. A similar structural propensity was found in presence of LPS micelles in the case of the synthetically designed β-boomerang peptide YI12 and the MSI-594 peptide, which is an α-helical peptide designed from magainin and melittin.[46, 47] The three active analogs of YI12 peptides (YI12WF, YI12WY, and YI12WW) formed a hydrophobic hub between Trp4 and Phe-9/Tyr-9/Trp-9, but the inactive YI12AA peptide showed a deficiency in hydrophobic-aromatic packing in the presence of LPS.[46] The importance of amphipathic structure and hydrophobic packing via the phenylalanine residue was also reported in case of MSI-594 and its mutant analog MSI-594F5A peptide where the F5A mutation completely disturbed the helical hairpin structure of MSI-594 in LPS micelles.[47, 48] The electrostatic potential map shown in Figure 3C supported both the amphipathicity as well as the compact bioactive conformation of the peptide. It is evident from the above two structures that how the peptide changes its random coil conformation to a defined amphipathic shape in the presence of bacterial outer and inner membrane environments as depicted by the overlaid structures shown in Figure 3D, that subsequently destabilizes the whole plasma membrane of this unicellular organism.

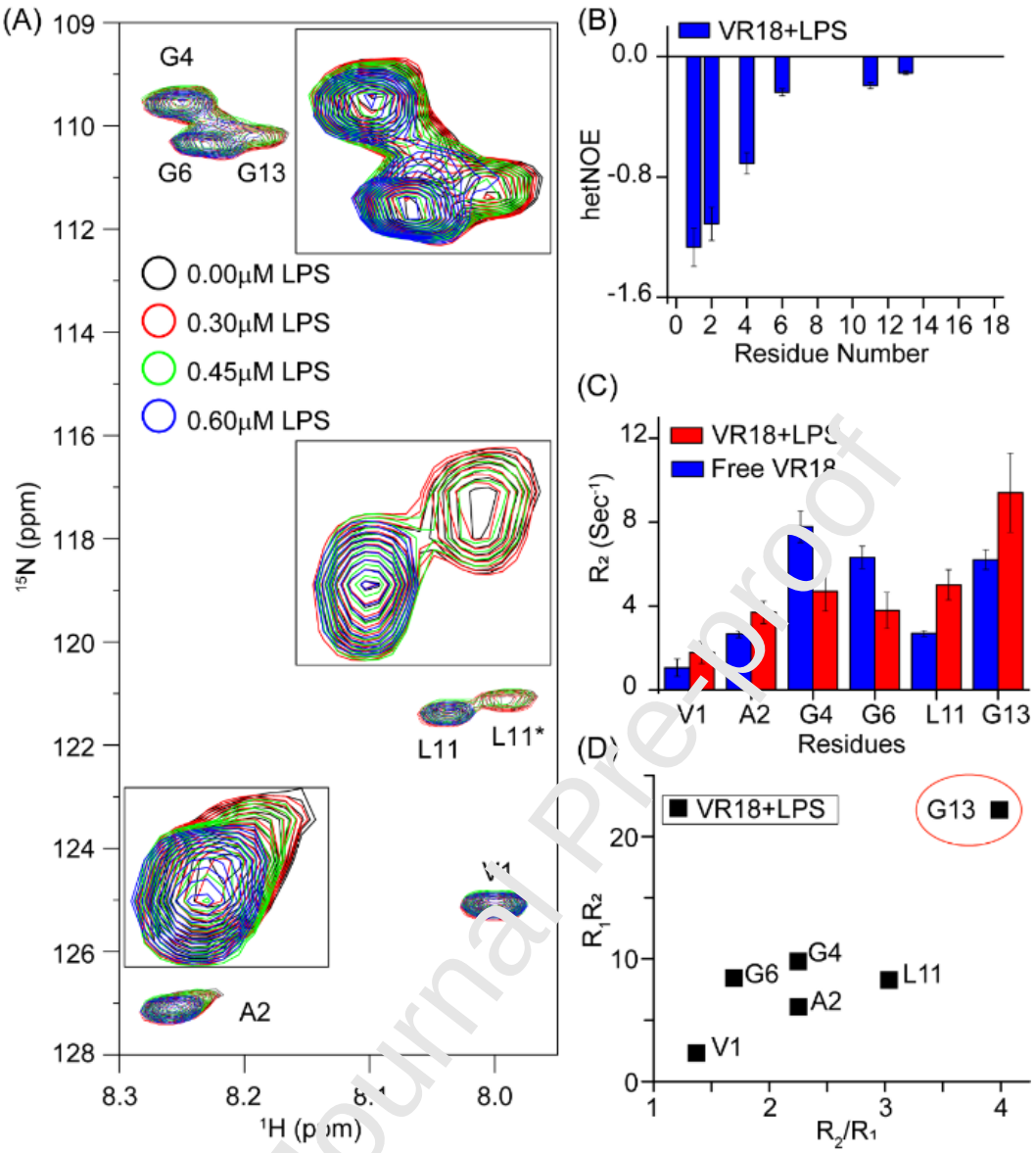

Figure 4. (A) Overlay of 2D ^{1}H-^{15}N-HSQC spectra of 1.0 mM ^{15}N-labelled VR18 peptide (at 298 K, pH 4.5) recorded upon titration with increasing concentrations of LPS (ranging from 0 to 0.6 µM). Residue specific assignment for each peak is marked on the spectrum. The amino acid sequence of the peptide is shown at the top of the HSQC spectrum with selectively ^{15}N-labelled residues (Val-1, Ala-2, Gly-4, Gly-6, Leu-11 and Gly-13) highlighted in blue. Except for Leu-11 residue, the exchange peaks for all other ^{15}N labelled residues were broadened and overlapping with the major conformational peak, whereas Leu11 clearly showed two cross peaks signifying largely different conformations exchanging slowly. The HSQC cross-peak of Leu-11 corresponding to minor conformational state have been highlighted in the spectrum by an asterisk (*). (B) The heteronuclear NOE plot of LPS bound VR18. (C) The R2 values of free and LPS bound VR18 peptide is shown in the bar plot. (D) The R_2/R_1 vs R_1R_2 plot of LPS bound VR18 depicting the level of molecular anisotropy and chemical exchange of each residue. The Gly-13 marked in the red circle is going through chemical exchange with LPS molecule. The error bars represent the ±SD.

Heteronuclear spin relaxation rates have been shown to be powerful probes of the general and internal dynamics of macromolecules.[49] To gain insight into the backbone dynamics of the LPS micelle bound VR18, the measurement of ^{1}H-^{15}N heteronuclear NOE (hetNOE), ^{15}N longitudinal ($R_1 = 1/T_1$) and transverse ($R_2 = 1/T_2$) relaxation rates were studied at 298 K. Out of 18 amino acid residues, six residues (Val-1, Ala-2, Gly-4, Gly-6, Leu-11, and Gly-13) were selectively labelled with ^{15}N via Fmoc chemistry and subsequent purification and mass was observed and compared with unlabeled VR18 via RP-HPLC and MALDI TOF analysis as shown in Figure S5.[50] The peptide-LPS interaction was observed by titrating 1 mM VR18 aqueous solution with increasing concentration of LPS (0.3, 0.45, 0.6 μM) from 1 mM stock solution, which resulted in a concentration-dependent broadening to the amide signals as shown in Figure 4A. Close inspection revealed that Leu-11 exhibited multiple amide cross-peaks in the HSQC spectrum (showed in inset), suggesting that there is a slow conformational exchange ($<<10^3$ sec^{-1}) between multiple conformations at the NMR time scale. This is probably due to the presence of Pro-10. The overlayed HSQC spectra of VR18 in the free state (black) and at increasing concentrations of LPS (red, green, and blue) (Figure 4A) revealed no significant chemical shift perturbation, implying that the peptide binding to LPS involves a rapid conformational exchange between the free and bound states on the NMR time scale. The intensity vs LPS concentration plot in Figure S6 revealed that the amide peak broadening of Gly-4 and Gly-13 is maximum, followed by Ala-2, Val-1, Gly-6, and Leu-11. The bulky LPS molecule interacts with the positively charged C-terminal KNKSR moiety and other Arg, Lys residues, so the close proximity of Gly-13 to KNKSR moiety and the Ala-2 and Gly-4 to Arg-3 resulted in an increased T_2 relaxation similar to LPS. Leu-11 might not be involved in an immediate association with LPS compared to the Gly-13/Gly-4/Ala-2. In other words, Leu-11 comes close to LPS after the peptide adopts a folded

conformation in LPS. Collectively, these results represent the systematic folding of VR18 in LPS micelles at an atomic resolution.

The flexibility of folded VR18 was estimated by measuring the hetNOE. The NOE value determined for each residue is plotted in Figure 4B. All the residues showed negative NOE with gradually increasing value from Val-1 (-1.27) to Gly-13 (-0.1). It suggests that the N-terminal end is more flexible than the C-terminal end in an overall dynamic structure. In parallel with the hetNOE, conformational flexibility of the individual residues is indicated by R_2 values. The non-polar residues (Val-1, Ala-2, and Leu-11) that took part in the hydrophobic cluster formation, and interacted with the acyl chains of the lipids, showed higher R_2 values than the free peptide as depicted in Figure 4C. The rotational correlation time of the individual residues corroborates with this finding, as shown in Figure S7A. Notwithstanding, the R_1 relaxation rates for most of the residues do not show significant changes (Figure S7B). Thus, to differentiate between the effects of residue-specific chemical exchange from the motional anisotropy in the complex formation, we plotted the product of the longitudinal and transverse relaxation rates that helped to accentuate the effect of the chemical exchange alone (Figure S7E-F). This difference with the R_2/R_1 plots (Figure S7C-D) corresponding to the rotational correlation time is particularly noteworthy in the free form with a high degree of molecular anisotropy. This, however, is largely abolished in the LPS-bound values. A significant difference was observed for Gly-13 in the LPS-bound complex.[14, 51] This suggests the contribution of chemical exchange over the rotational anisotropy. Thus, the plot of $R_2.R_1$ vs R_2/R_1 (Figure 4D) helps represent the partitioning between residues directly affected by chemical exchange at the interaction interface. The data reinstates the direct involvement of the C-terminal KNKSR moiety in binding firmly to the LPS phosphate head groups.

Evaluation of the in vitro, ex vivo and in vivo efficacy of VR18 peptide

In order to find the structure-function correlation, and study the protective effect of the peptide against *P. aeruginosa*, HCEC were infected with PAO1 for 4 h in presence or absence of the peptide. Microscopic images in Figure 5A showed that the VR18-treated HCEC cells were more viable than the untreated cells in presence of PAO1, which was correlated with the bacterial vaibility as obtained from optical density measurement (OD_{600}) (Figure 5B). The reduced cell death of HCEC was evident from the lowered LDH release in presence of increasing concentration of VR18 (Figure 5C) which suggests that VR18 renders protection to the HCEC cells infected with PAO1.

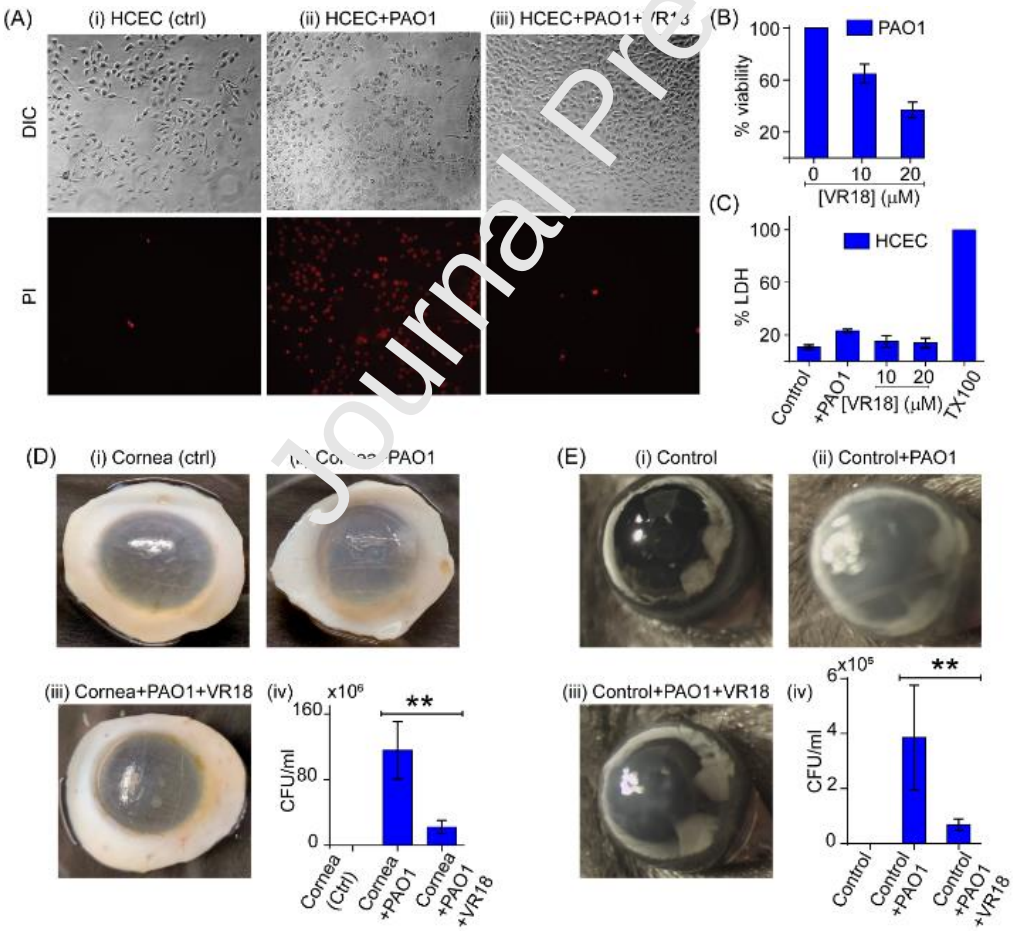

Figure 5. (A) The microscopic study showed that the Control HCEC cells along with PAO1 infected cells in DIC and PI channel. The addition of 10 and 20 μM VR18 had little impact on the viability of the HCEC cells. (B) The percentage of the viable PAO1 population was decreased with increasing concentration of VR18. (C) Percentage release of LDH enzyme from PAO1 infected and VR18 treated cells compared with positive control. (D) (i-iii) The *ex vivo* infection model of PAO1 was performed using the human corneas where the infected cornea showed an opaque condition but the VR18 treated cornea showed quite transparent appearance similar to the control set. (D) (iv) The CFU/ml count showed a drastic change in presence of VR18. (E) (i-iii) *in vivo* keratitis infection model where *P. aeruginosa* PAO1 was used as the causative agent. The control untreated eye showed clear cornea (i), the PAO1 infected eye showed severely opaque cornea (ii), The iris and lens and the VR18 (50μM) treated eye showed moderately opaque cornea where iris and lens are still detectable (iii). (E) (iv) The CFU of PAO1 cells obtained after the treatment. (*P < 0.01. **P < 0.001. N.S- Not significant).

The efficacy of the peptide was further determined using our *ex vivo* infection model [31, 52] using human cadaveric corneas. The corneas were scratched and infected with 10^5 CFU/ml of PAO1 in presence or absence of 50 μM VR18 peptide (n=3). 24 h post infection, corneas were washed with PBS, imaged and homogenized and bacterial load was determined by serial dilutions. There were reduced corneal opacity in corneas treated with the peptide along with significantly reduced bacterial colony forming units (CFU) (Figure 5D (i-iv)).

The effect of VR18 was further determined *in vivo*, using our established murine model of keratitis [31, 52] in which corneas of C57BL/6 mice were scratched and infected with PAO1 and treated topically with VR18 (50 μM) at 0, and 6 h post-infection. Animals were euthanized after 24 h and corneas were imaged for opacification, and viable *P. aeruginosa* in whole eyes were quantified by CFU after enucleation. Increased corneal opacity was detected in mice infected with PAO1 (Figure 5E (ii)), but significantly less opacity was observed in infected mice treated with VR18 (Figure 5E (iii)). Consistent with this data, CFU per eye obtained from VR18 treated corneas were lower than the ones infected with PAO1 (Figure 5E (iv)). The efficacy of the peptide was also tested against *P. aeruginsa* 6294 strain *in vivo*, and similar results were obtained (data not shown). In the next step, a multiplex ELISA assay was performed to check the

effect of the peptide on the inflammatory cytokines or chemokines. Increased secretion of IL-8, CXCL5, CCL5 and VEGF were observed in cells infected with PAO1 in the presence of VR18, indicating its immunomodulatory role (Figure S8). This is an interesting finding which needs to be explored further to reveal the role of the peptide with expression of cell signalling factors in HCEC.

VR18 induces generation of reactive oxygen species (ROS)

The results, thus far, indicate that VR18 interacts with *P. aeruginsa* cells which induces bacterial cell death. However, little is known about how VR18 induces toxicity in *P. aeruginsa*. Previous studies have shown that antimicrobial stress in the presence of antibiotics or AMPs stimulates the generation of intracellular reactive oxygen species (ROS), resulting in bacterial cell death. Hydroxyl radicals, superoxide, hydrogen peroxide, which make up the majority of reactive oxygen species (ROS), cause intracellular damage by oxidizing GTP and CTP pools, as well as causing double-stranded DNA breaks. ROS-induced damage is secondary to the main stress-mediated injury, and this could activate subsequent ROS deposition rounds, resulting in stress-induced bacterial cell death.[34, 5] Based on these studies, we hypothesized that VR18 induced toxic effects on *P. aeruginosa* trigger oxidative stress and ROS generation in bacterial cells. To test this hypothesis, we measured the ROS generation in *P. aeruginosa* in the presence of VR18. Interestingly, we found that the application of the VR18 to *P. aeruginosa* loaded with the ROS-sensing dye, CM-H2DCFDA produced a drastic increase in ROS production (Figure 6A-D; Supplementary Video S1). To further validate this finding, as a control, the membrane-permeable oxidant "tertbutyl hydrogen peroxide (tbH_2O_2)" was applied. This showed an increase in intracellular ROS levels in *P. aeruginosa* while the application of buffer alone did not display any sensitivity towards ROS generation (Figure S9). This observation suggests that the

generation of ROS may be the secondary mechanism by which VR18 contributes to the VR18 mediated killing of *P. aeruginosa*. Further, our study showed that topical application of VR18 can significantly reduce keratitis in *in vivo* animal model. This applies that the *in vitro* observations are in direct agreement with clinical observations. Thus, VR18 can be considered as a highly potent therapeutic agent for treatment and management for *Pseudomonas* associated keratitis.

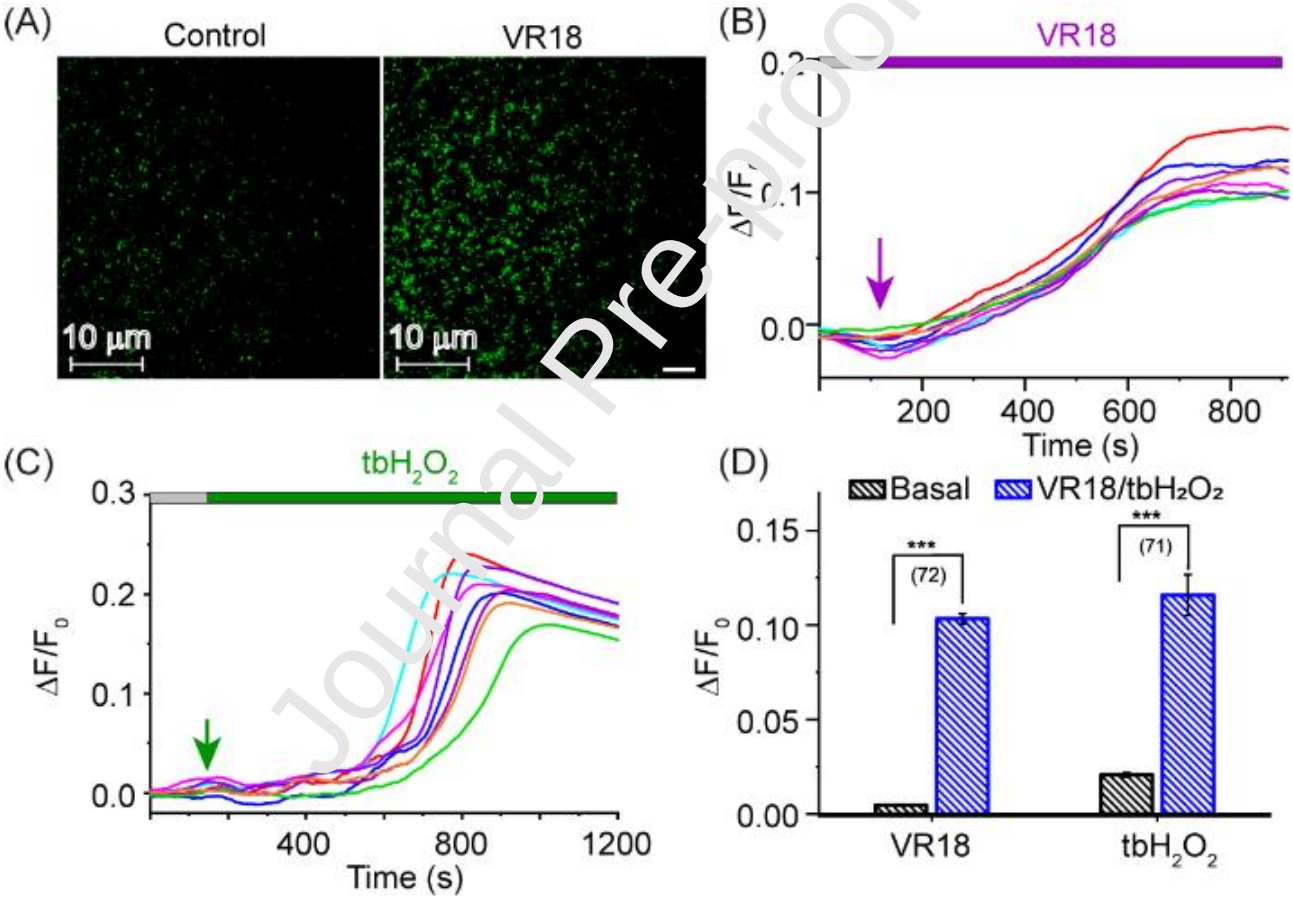

Figure 6. VR18 induces ROS generation in *Pseudomonas aeruginosa.* (A) Representative fluorescence microscopy image of *P. aeruginosa* at 100x magnification. *P. aeruginosa* was loaded with ROS sensing dye CM-H_2DCFDA before (left) and after 450 s of VR18 application. (B-C) Representative ROS imaging trace showing an increase in ROS level upon application of VR18 (B) and tbH_2O_2 (C). Each ROS imaging trace shown in (B, C) represents average fluorescence intensity of ~20-50 *P. aeruginosa* bacteria (D) Bar graph analysis of data shown in (B) and (C) depicting the maximum ROS generation after VR18 and tbH_2O_2 application. Statistical indicators reflect the t-test, measuring for an effect of VR18 and tbH_2O_2 on ROS production: ***P < 0.0001. The parentheses number in (D) represents the ROS imaging trace obtained from 2-3 independent measurements. Scale bar: 10 µm.

CONCLUSION

In summary, the hybrid antimicrobial peptide VR18 has high potency against *Pseudomonas aeruginosa* clinical isolates supported by *in vitro* experiments. The results of the *in vivo* studies are in agreement with the *in vitro* measurements. The biophysical analysis and the dynamics of the VR18 peptide indicate membrane specificity towards the microbial membrane over the mammalian membrane. Together with our previous report, it can be concluded that the mode of action of the VR18 peptide is through membrane lysis via an electrostatic interaction with negatively charged lipids and subsequent hydrophobic interactions. This mediates pore formation in the microbial cells as observed in the dye leakage assay and vesicle disruption in phase contrast microscopic analysis. We further tested its modes of action using live-cell NMR, Raman spectroscopy and sparsely tethered bilayer lipid membranes. We have also shown that VR18 has little toxicity against human corneal epithelial cells. As VR18 has high potency against *Pseudomonas aeruginosa*, as shown by *in vitro, ex vivo* and *in vivo* experiments, we conclude it has the potential to be used clinically for the treatment and prevention of corneal keratitis.

ASSOCIATED CONTENT

Supporting Information. Raman spectra analysis of live *Pseudomonas aeruginosa* in the absence and presence of VR18 (Table S1); Thermodynamic analysis of VR18-LPS interaction (Table 2); Composition of *E.coli* total lipid extract (Table 3); Structural statistics of VR18 in the presence of two different membrane composition (Table S4); Cell membrane permeabilization and Live cell NMR experiments (Figure S1); ITC analysis and CD data (Figure S2); Selected trNOESY spectra of VR18 in the presence of LPS bicelle (Figure S3); Bar and histogram plot of

VR18 in two different membrane composition (Figure S4); Characterization of purity of peptide by HPLC and MS (Figure S5); Analysis of ^{15}N-labeled amino acids of VR18 in the presence of LPS from 2D Sofast HSQC spectra (Figure S6); Residue specific relaxation data of VR18 in the absence and presence of VR18 (Figure S7); Signaling pathway analysis data of cells infected with *Pseudomonas aeruginosa* PAO1 in the absence and presence of VR18 (Figure S8); Control data of live cell microscopy (Figure S9); Live cell microscopy video (Supplementary Video S1).

AUTHOR INFORMATION

Corresponding Author

* Corresponding E-mail: anirbanbhunia@gmail.com / bhunia@jcbose.ac.in

Author Contributions

AB conceived the project and designed the research; SAM performed biophysical assays, solution- and solid-state NMR experiments; SAM and SR did live cell Raman spectroscopy under the guidance of AS; SAM and KA did zeta potential experiments; PS did *in vitro*, *in vivo* and *ex vivo* experiments with SR; TS and NS did live cell microscopy experiments; AA performed tethered bilayer lipid membranes experiments under the supervision of CGC; DD and MDPW did *in vivo* experiments; SAM and AB analyzed solution-state NMR data; DKL analyzed solid-state NMR data; SAM, CGC, SR and AB wrote the manuscript; all authors reviewed the manuscript; AB arranged the funding for this work.

Funding Sources

This research was partly supported by Science and Engineering Research Board, Govt. of India (File No. EMR/2017/003457 to AB), and partly by Bose Institute intramural external research fund (to AB); NIH Grant, USA (SC2GM139715) to NS and National Research Foundation of

Korea (NRF) funded by the Ministry of Education (Grants No. NRF-2020R1A6A1A03042742) to DKL.

NOTES

The atomic coordinates and structure factors (PDB IDs: 7VQI and 7VQH) have been deposited in the Protein Data Bank (http://wwpdb.org/). The three-dimensional *P. aeruginosa* LPS and *E. coli* TLE bicelle-bound structures of the VR18 peptide have been submitted to Biological Magnetic Resonance Data Bank (BMRB). The BMRB code for *P. aeruginosa* LPS and *E. coli* TLE bicelle-bound structures of the VR18 peptide are 36451 and 36450, respectively.

ACKNOWLEDGMENT

SAM acknowledges Bose Institute for Senior Research Fellowship. AB would like to thank Dr. Nakul C. Maiti CSIR-IICB, India for discussion on Raman data analysis.

ABBREVIATIONS

AMP: Antimicrobial peptide, NMR: Nuclear magnetic Resonance, LPS: Lipopolysaccharides, PI: Propidium iodide, ROS: Reactive oxygen species, OD: Optical density, NOE: Nuclear Overhauser effect, TOCSY: Total correlation spectroscopy, NOESY: Nuclear Overhauser effect spectroscopy, *tr*NOESY: transferred Nuclear Overhauser effect spectroscopy ALS: asymmetric least squares, LUV: Large unilamellar vesicle, GUV: Giant unilamellar vesicle, ITC: Isothermal titration calorimetry, $MIC_{99\%}$: Minimal inhibitory concentration for 99% killing, HSQC: heteronuclear single quantum correlation, HCEC: Human corneal epithelial cells, MTT: (3-(4,5-

Dimethylthiazol-2-yl)-2,5-Diphenyltetrazolium Bromide), POPE: 1-palmitoyl-2-oleoyl-sn-glycero-3-phosphoethanolamine, POPG: 1-palmitoyl-2-oleoyl-sn-glycero-3-phospho-(1-rac-glycerol), CHAPSO: 3-[(3-cholamidopropyl)dimethylammonio]-2-hydroxy-1-propanesulfonic acid, TSP: 3-(trimethylsilyl)propionic-2,2,3,3-*d*4 acid sodium salt, CFU: Colony forming unit

REFERENCES

(1) Ting, D. S. J.; Ho, C. S.; Deshmukh, R.; Said, D. G.; Dua, H. S. Infectious keratitis: an update on epidemiology, causative microorganisms, risk factors, and antimicrobial resistance. *Eye (Lond)* **2021**, *35* (4), 1084-1101. DOI: 10.1038/s41433-020-01339-3.
(2) Li, N.; Zhu, Z.; Yi, G.; Li, S.; Han, X. Corneal Opacity Leading to Multiple Myeloma Diagnosis: A Case Report and Literature Review. *Am J Case Rep* **2018**, *19*, 421-425. DOI: 10.12659/ajcr.908475.
(3) Taylor, H. R.; Burton, M. J.; Haddad, D.; West, S.; Wright, H. Trachoma. *Lancet* **2014**, *384* (9960), 2142-2152. DOI: 10.1016/S0140-6736(13)62182-0.
(4) Austin, A.; Lietman, T.; Rose-Nussbaumer, J. Update on the Management of Infectious Keratitis. *Ophthalmology* **2017**, *124* (11), 1678-1689. DOI: 10.1016/j.ophtha.2017.05.012. Kam, K. W.; Yung, W.; Li, G. K. H.; Chen, L. J.; Young, A. L. Infectious keratitis and orthokeratology lens use: a systematic review. *Infection* **2017**, *45* (6), 727-735. DOI: 10.1007/s15010-017-1023-2.
(5) Aydin, B.; Cubuk, M. O.; Ucgul, A.; Ertop, M.; Ozmen, M. C.; Atalay, T.; Akata, F. Combined Intrastromal Voriconazole and Amphotericin B Treatment for Persistent Fungal Keratitis. *Eye Contact Lens* **2020**, *46* (5), 269-273. DOI: 10.1097/ICL.0000000000000723. Chang, V. S.; Dhaliwal, D. K.; Rain, L.; Kowalski, R. P. Antibiotic Resistance in the Treatment of Staphylococcus aureus Keratitis: a 20-Year Review. *Cornea* **2015**, *34* (6), 698-703. DOI: 10.1097/ICO.0000000000000431.
(6) Barceló-Vidal, J.; Rodríguez García, E.; Grau, S. Extremely high levels of vancomycin can cause severe renal toxicity. *Infect Drug Resist* **2018**, *11*, 1027-1030. DOI: 10.2147/IDR.S171669. Hamill, R. J. Amphotericin B formulations: a comparative review of efficacy and toxicity. *Drugs* **2013**, *73* (9), 919-934. DOI: 10.1007/s40265-013-0069-4.
(7) Nikaido, H. Multidrug resistance in bacteria. *Annu Rev Biochem* **2009**, *78*, 119-146. DOI: 10.1146/annurev.biochem.78.082907.145923. Lakshminarayanan, R.; Ye, E.; Young, D. J.; Li, Z.; Loh, X. J. Recent Advances in the Development of Antimicrobial Nanoparticles for Combating Resistant Pathogens. *Adv Healthc Mater* **2018**, *7* (13), e1701400. DOI: 10.1002/adhm.201701400.
(8) Bechinger, B.; Gorr, S. U. Antimicrobial Peptides: Mechanisms of Action and Resistance. *J Dent Res* **2017**, *96* (3), 254-260. DOI: 10.1177/0022034516679973.
(9) Sani, M. A.; Separovic, F. How Membrane-Active Peptides Get into Lipid Membranes. *Acc Chem Res* **2016**, *49* (6), 1130-1138. DOI: 10.1021/acs.accounts.6b00074.
(10) Haney, E. F.; Mansour, S. C.; Hancock, R. E. Antimicrobial Peptides: An Introduction. *Methods Mol Biol* **2017**, *1548*, 3-22. DOI: 10.1007/978-1-4939-6737-7_1. Lazzaro, B. P.; Zasloff, M.; Rolff, J. Antimicrobial peptides: Application informed by evolution. *Science* **2020**, *368* (6490). DOI: 10.1126/science.aau5480.

(11) Sani, M. A.; Separovic, F. Antimicrobial Peptide Structures: From Model Membranes to Live Cells. *Chemistry* **2018**, *24* (2), 286-291. DOI: 10.1002/chem.201704362. Malmsten, M. Antimicrobial peptides. *Ups J Med Sci* **2014**, *119* (2), 199-204. DOI: 10.3109/03009734.2014.899278.
(12) Ilyas, H.; Kim, J.; Lee, D.; Malmsten, M.; Bhunia, A. Structural insights into the combinatorial effects of antimicrobial peptides reveal a role of aromatic-aromatic interactions in antibacterial synergism. *J Biol Chem* **2019**, *294* (40), 14615-14633. DOI: 10.1074/jbc.RA119.009955.
(13) Mohid, S. A.; Ghorai, A.; Ilyas, H.; Mroue, K. H.; Narayanan, G.; Sarkar, A.; Ray, S. K.; Biswas, K.; Bera, A. K.; Malmsten, M.; et al. Application of tungsten disulfide quantum dot-conjugated antimicrobial peptides in bio-imaging and antimicrobial therapy. *Colloids Surf B Biointerfaces* **2019**, *176*, 360-370. DOI: 10.1016/j.colsurfb.2019.01.020.
(14) Datta, A.; Jaiswal, N.; Ilyas, H.; Debnath, S.; Biswas, K.; Kumar, D.; Bhunia, A. Structural and Dynamic Insights into a Glycine-Mediated Short Analogue of a Designed Peptide in Lipopolysaccharide Micelles: Correlation Between Compact Structure and Anti-Endotoxin Activity. *Biochemistry* **2017**, *56* (9), 1348-1362. DOI: 10.1021/acs.biochem.6b01229.
(15) Halder, S.; Yadav, K. K.; Sarkar, R.; Mukherjee, S.; Saha, P.; Haldar, S.; Karmakar, S.; Sen, T. Alteration of Zeta potential and membrane permeability in bacteria: a study with cationic agents. *Springerplus* **2015**, *4*, 672. DOI: 10.1186/s40064-015-1476-7.
(16) Ratha, B. N.; Kar, R. K.; Bednarikova, Z.; Gazova, Z.; Kotler, S. A.; Raha, S.; De, S.; Maiti, N. C.; Bhunia, A. Molecular Details of a Salt Bridge and Its Role in Insulin Fibrillation by NMR and Raman Spectroscopic Analysis. *J Phys Chem B* **2020**, *124* (7), 1125-1136. DOI: 10.1021/acs.jpcb.9b10349.
(17) Jung, G. B.; Nam, S. W.; Choi, S.; Lee, G. J.; Park, H. K. Evaluation of antibiotic effects on Pseudomonas aeruginosa biofilm using Raman spectroscopy and multivariate analysis. *Biomed Opt Express* **2014**, *5* (9), 3238-3251. DOI: 10.1364/BOE.5.003238.
(18) Patel, K. D.; Mohid, S. A.; Datta, A.; Arichthota, S.; Bhunia, A.; Haldar, D.; Sarojini, V. Synthesis and antibacterial study of cell-penetrating peptide conjugated trifluoroacetyl and thioacetyl lysine modified peptides. *Eur J Med Chem* **2021**, *219*, 113447. DOI: 10.1016/j.ejmech.2021.113447.
(19) Weinberger, A.; Tsai, F. C.; Koenderink, G. H.; Schmidt, T. F.; Itri, R.; Meier, W.; Schmatko, T.; Schröder, A.; Marques, C. Gel-assisted formation of giant unilamellar vesicles. *Biophys J* **2013**, *105* (1), 154-164. DOI: 10.1016/j.bpj.2013.05.024.
(20) Mescola, A.; Marín Medina, N.; Ragazzini, G.; Accolla, M.; Alessandrini, A. Magainin-H2 effects on the permeabilization and mechanical properties of giant unilamellar vesicles. *J Colloid Interface Sci* **2019**, *553*, 247-258. DOI: 10.1016/j.jcis.2019.06.028.
(21) Cranfield, C. G.; Henriques, S. T.; Martinac, B.; Duckworth, P.; Craik, D. J.; Cornell, B. Kalata B1 and Kalata B2 Have a Surfactant-Like Activity in Phosphatidylethanolomine-Containing Lipid Membranes. *Langmuir* **2017**, *33* (26), 6630-6637. DOI: 10.1021/acs.langmuir.7b01642.
(22) Cranfield, C.; Carne, S.; Martinac, B.; Cornell, B. The assembly and use of tethered bilayer lipid membranes (tBLMs). *Methods Mol Biol* **2015**, *1232*, 45-53. DOI: 10.1007/978-1-4939-1752-5_4.
(23) Cranfield, C. G.; Bettler, T.; Cornell, B. Nanoscale ion sequestration to determine the polarity selectivity of ion conductance in carriers and channels. *Langmuir* **2015**, *31* (1), 292-298. DOI: 10.1021/la504057z.

(24) Varnava, K. G.; Mohid, S. A.; Calligari, P.; Stella, L.; Reynison, J.; Bhunia, A.; Sarojini, V. Design, Synthesis, Antibacterial Potential, and Structural Characterization of N-Acylated Derivatives of the Human Autophagy 16 Polypeptide. *Bioconjug Chem* **2019**, *30* (7), 1998-2010. DOI: 10.1021/acs.bioconjchem.9b00290.
(25) Roumestand, C.; Canet, D. Extending the excitation sculpting concept for selective excitation. *J Magn Reson* **2000**, *147* (2), 331-339. DOI: 10.1006/jmre.2000.2206.
(26) *Sparky*; University of California: San Francisco, (accessed.
(27) Datta, A.; Bhattacharyya, D.; Singh, S.; Ghosh, A.; Schmidtchen, A.; Malmsten, M.; Bhunia, A. Role of Aromatic Amino Acids in Lipopolysaccharide and Membrane Interactions of Antimicrobial Peptides for Use in Plant Disease Control. *J Biol Chem* **2016**, *291* (25), 13301-13317. DOI: 10.1074/jbc.M116.719575.
(28) Bhattacharyya, D.; Kim, M.; Mroue, K. H.; Park, M.; Tiwari, A.; Saleem, M.; Lee, D.; Bhunia, A. Role of non-electrostatic forces in antimicrobial potency of a dengue-virus derived fusion peptide VG16KRKP: Mechanistic insight into the interfacial peptide-lipid interactions. *Biochim Biophys Acta Biomembr* **2019**, *1861* (4), 798-809. DOI: 10.1016/j.bbamem.2019.01.011.
(29) Güntert, P.; Mumenthaler, C.; Wüthrich, K. Torsion angle dynamics for NMR structure calculation with the new program DYANA. *J Mol Biol* **1997**, *273* (1), 283-298. DOI: 10.1006/jmbi.1997.1284.
(30) Laskowski, R. A.; Rullmannn, J. A.; MacArthur, M. W.; Kaptein, R.; Thornton, J. M. AQUA and PROCHECK-NMR: programs for checking the quality of protein structures solved by NMR. *J Biomol NMR* **1996**, *8* (4), 477-486.
(31) Sharma, P.; Elofsson, M.; Roy, S. Attenuation of. *Virulence* **2020**, *11* (1), 795-804. DOI: 10.1080/21505594.2020.1776979.
(32) Sharma, P.; Sharma, N.; Mishra, P., Joseph, J.; Mishra, D. K.; Garg, P.; Roy, S. Differential Expression of Antimicrobial Peptides in Streptococcus pneumoniae Keratitis and STAT3-Dependent Expression of LL-37 by Streptococcus pneumoniae in Human Corneal Epithelial Cells. *Pathogens* **2019**, *8* (1). DOI: 10.3390/pathogens8010031.
(33) Hong, Y.; Zeng, J.; Wang, X.; Drlica, K.; Zhao, X. Post-stress bacterial cell death mediated by reactive oxygen species. *Proc Natl Acad Sci U S A* **2019**, *116* (20), 10064-10071. DOI: 10.1073/pnas.1901730116.
(34) Su, L. J.; Zhang, J. H.; Gomez, H.; Murugan, R.; Hong, X.; Xu, D.; Jiang, F.; Peng, Z. Y. Reactive Oxygen Species-Induced Lipid Peroxidation in Apoptosis, Autophagy, and Ferroptosis. *Oxid Med Cell Longev* **2019**, *2019*, 5080843. DOI: 10.1155/2019/5080843.
(35) Sawa, T.; Ohara, M.; Kurahashi, K.; Twining, S. S.; Frank, D. W.; Doroques, D. B.; Long, T.; Gropper, M. A.; Wiener-Kronish, J. P. In vitro cellular toxicity predicts Pseudomonas aeruginosa virulence in lung infections. *Infect Immun* **1998**, *66* (7), 3242-3249. DOI: 10.1128/IAI.66.7.3242-3249.1998. Kugadas, A.; Christiansen, S. H.; Sankaranarayanan, S.; Surana, N. K.; Gauguet, S.; Kunz, R.; Fichorova, R.; Vorup-Jensen, T.; Gadjeva, M. Impact of Microbiota on Resistance to Ocular Pseudomonas aeruginosa-Induced Keratitis. *PLoS Pathog* **2016**, *12* (9), e1005855. DOI: 10.1371/journal.ppat.1005855.
(36) Kłodzińska, E.; Szumski, M.; Dziubakiewicz, E.; Hrynkiewicz, K.; Skwarek, E.; Janusz, W.; Buszewski, B. Effect of zeta potential value on bacterial behavior during electrophoretic separation. *Electrophoresis* **2010**, *31* (9), 1590-1596. DOI: 10.1002/elps.200900559.
(37) Bridges, D. F.; Lacombe, A.; Wu, V. C. H. Integrity of the. *Front Microbiol* **2020**, *11*, 888. DOI: 10.3389/fmicb.2020.00888.

(38) Kasibhatla, S.; Amarante-Mendes, G. P.; Finucane, D.; Brunner, T.; Bossy-Wetzel, E.; Green, D. R. Propidium Iodide (PI) Uptake Assay to Detect Apoptosis. *CSH Protoc* **2006**, *2006* (2). DOI: 10.1101/pdb.prot4495.
(39) Datta, A.; Ghosh, A.; Airoldi, C.; Sperandeo, P.; Mroue, K. H.; Jiménez-Barbero, J.; Kundu, P.; Ramamoorthy, A.; Bhunia, A. Antimicrobial Peptides: Insights into Membrane Permeabilization, Lipopolysaccharide Fragmentation and Application in Plant Disease Control. *Sci Rep* **2015**, *5*, 11951. DOI: 10.1038/srep11951.
(40) Pahlow, S.; Meisel, S.; Cialla-May, D.; Weber, K.; Rösch, P.; Popp, J. Isolation and identification of bacteria by means of Raman spectroscopy. *Adv Drug Deliv Rev* **2015**, *89*, 105-120. DOI: 10.1016/j.addr.2015.04.006.
(41) Chowdhury, R.; Ilyas, H.; Ghosh, A.; Ali, H.; Ghorai, A.; Midya, A.; Jana, N. R.; Das, S.; Bhunia, A. Multivalent gold nanoparticle-peptide conjugates for targeting intracellular bacterial infections. *Nanoscale* **2017**, *9* (37), 14074-14093. DOI: 10.1039/c7nr04062h.
(42) Schiller, J.; Muller, M.; Fuchs, B.; Arnold, K.; Huster, D. 31P NMR Spectroscopy of Phospholipids: From Micelles to Membranes. *Current Analytical Chemistry* **2007**, *3* (4), 283-301. DOI: http://dx.doi.org/10.2174/157341107782109635
(43) Mason, A. J.; Marquette, A.; Bechinger, B. Zwitterionic phospholipids and sterols modulate antimicrobial peptide-induced membrane destabilization. *Biophys J* **2007**, *93* (12), 4289-4299. DOI: 10.1529/biophysj.107.116681.
(44) Meikle, T. G.; Conn, C. E.; Separovic, F.; Drummond, C. J. Exploring the structural relationship between encapsulated antimicrobial peptides and the bilayer membrane mimetic lipidic cubic phase: studies with gramicidin A. *RSC Advances* **2016**, *6* (73), 68685-68694, 10.1039/C6RA13658C. DOI: 10.1039/C6RA13658C. Mankoci, S.; Ewing, J.; Dalai, P.; Sahai, N.; Barton, H. A.; Joy, A. Bacterial Membrane Selective Antimicrobial Peptide-Mimetic Polyurethanes: Structure-Property Correlations and Mechanisms of Action. *Biomacromolecules* **2019**, *20* (11), 4096-4106. DOI: 10.1021/acs.biomac.9b00939.
(45) Biswas, K.; Ilyas, H.; Datta, A.; Bhunia, A. NMR Assisted Antimicrobial Peptide Designing: Structure Based Modifications and Functional Correlation of a Designed Peptide VG16KRKP. *Curr Med Chem* **2020**, *27* (9), 1387-1404. DOI: 10.2174/0929867326666190624090817.
(46) Bhunia, A.; Mohanram, H.; Domadia, P. N.; Torres, J.; Bhattacharjya, S. Designed beta-boomerang antiendotoxic and antimicrobial peptides: structures and activities in lipopolysaccharide. *J Biol Chem* **2009**, *284* (33), 21991-22004. DOI: 10.1074/jbc.M109.013573.
(47) Bhunia, A.; Ramamoorthy, A.; Bhattacharjya, S. Helical hairpin structure of a potent antimicrobial peptide MSI-594 in lipopolysaccharide micelles by NMR spectroscopy. *Chemistry* **2009**, *15* (9), 2036-2040. DOI: 10.1002/chem.200802635.
(48) Domadia, P. N.; Bhunia, A.; Ramamoorthy, A.; Bhattacharjya, S. Structure, interactions, and antibacterial activities of MSI-594 derived mutant peptide MSI-594F5A in lipopolysaccharide micelles: role of the helical hairpin conformation in outer-membrane permeabilization. *J Am Chem Soc* **2010**, *132* (51), 18417-18428. DOI: 10.1021/ja1083255.
(49) Shukla, V. K.; Siemons, L.; Gervasio, F. L.; Hansen, D. F. Aromatic side-chain flips orchestrate the conformational sampling of functional loops in human histone deacetylase 8. *Chem Sci* **2021**, *12* (27), 9318-9327. DOI: 10.1039/d1sc01929e. Pritchard, R. B.; Hansen, D. F. Characterising side chains in large proteins by protonless. *Nat Commun* **2019**, *10* (1), 1747. DOI: 10.1038/s41467-019-09743-4.

(50) Chan, W. C.; White, P. D.; Beythien, J.; Steinauer, R. Facile synthesis of protected C-terminal peptide segments by Fmoc/But solid-phase procedures on N-Fmoc-9-amino-xanthen-3-yloxymethyl polystyrene resin. *Journal of the Chemical Society, Chemical Communications* **1995**, (5), 589-592, 10.1039/C39950000589. DOI: 10.1039/C39950000589.
(51) Kneller, J. M.; Lu, M.; Bracken, C. An effective method for the discrimination of motional anisotropy and chemical exchange. *J Am Chem Soc* **2002**, *124* (9), 1852-1853. DOI: 10.1021/ja017461k.
(52) Sun, Y.; Karmakar, M.; Roy, S.; Ramadan, R. T.; Williams, S. R.; Howell, S.; Shive, C. L.; Han, Y.; Stopford, C. M.; Rietsch, A.; et al. TLR4 and TLR5 on corneal macrophages regulate Pseudomonas aeruginosa keratitis by signaling through MyD88-dependent and -independent pathways. *J Immunol* **2010**, *185* (7), 4272-4283. DOI: 10.4049/jimmunol.1000874.
(53) Gandhi, A.; Kariyat, R. R.; Chappa, C.; Tayal, M.; Sahoo, N. Tobacco Hornworm (*Int J Mol Sci* **2020**, *21* (21). DOI: 10.3390/ijms21218297.

GRAPHICAL ABSTRACT

Corneal infections upon contact lens wear are a major health concern and a tough challenge for the eye care practitioners. Currently, there is no other alternative to topical antibiotic therapy or daily disposable lens except for corneal transplantation. Here, we report the topical employ of non-toxic and non-hemolytic VR18 as a powerful therapeutic agent for the prevention or remedy of Pseudomonas-associated microbial keratitis.

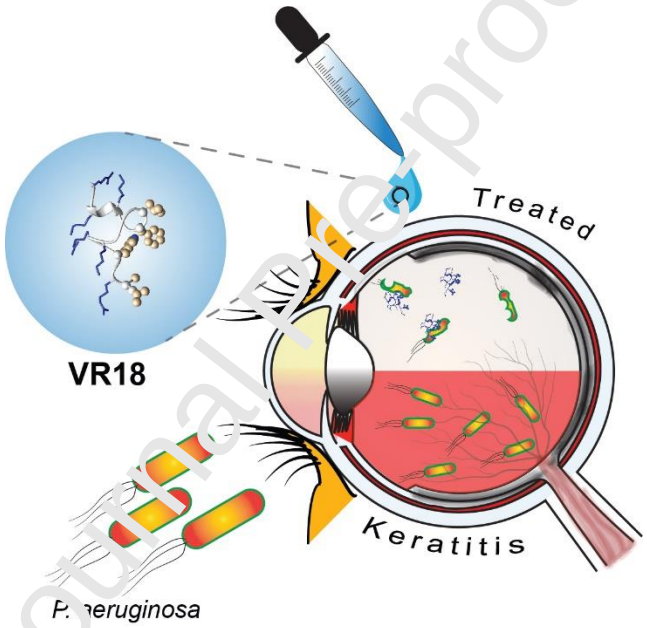

Institute and/or researcher Twitter usernames: @BhuniaLab

Highlights

- A hybrid antimicrobial peptide VR18 has high potency against *Pseudomonas aeruginosa* clinical isolates.
- VR18 peptide showed low toxicity to human derived HCEC cells.
- The biophysical analysis and the dynamics of the VR18 peptide indicate membrane specificity towards the microbial membrane over the mammalian membrane.
- We have tested the modes of action of VR18 using live-cell NMR, Raman spectroscopy and sparsely tethered bilayer lipid membranes.
- VR18 has the potential to be used clinically for the treatment and prevention of corneal keratitis.